SLAC – PUB – 4431
UTHEP – 87 – 0901
RAL – 87 – 078
September 1987
(T/E)

Production and Decay Properties of the $\omega\pi^0$ state at 1250 MeV/c^2 Produced by 20 GeV Polarized Photons on Hydrogen *

SLAC Hybrid Facility Photon Collaboration

J.E. Brau[q], B. Franek[j], W. Wester[q¶], K. Abe[m], T.C. Bacon[e], J. Ballam[k], H.H. Bingham[o], K. Braune[k◇], D. Brick[b], W.M. Bugg[q], J.M. Butler[k◇], W. Cameron[e], J.T. Carroll[k‡], C.V. Cautis[k], H.O. Cohn[i], D.C. Colley[a], G.T.Condo[q], S. Dado[l], R. Diamond[d†], P. Dingus[o], R. Erickson[k], T. Fieguth[k], R.C. Field[k], L. Fortney[c], B. Franek[j], N. Fujiwara[h], R. Gearhart[k], T. Glanzman[k], I.M. Godfrey[e], J.J. Goldberg[l], A.T. Goshaw[c], G. Hall[e], E.R. Hancock[j], T. Handler[q], H.J. Hargis[q], E.L. Hart[q], M.J. Harwin[e], K. Hasegawa[m], R.I. Hulsizer[g], M. Jobes[a], T. Kafka[n], G.E. Kalmus[j], D.P. Kelsey[j], J. Kent[o§], T. Kitagaki[m], A. Levy[p], W.A. Mann[n], R. Merenyi[n♮], R. Milburn[n], C. Milstene[p], E. McCrory[c‡], K.C. Moffeit[k], A. Napier[n], S. Noguchi[h], F. Ochiai[f], V.R. O'Dell[b], S. O'Neale[a], A.P.T. Palounek[g], I.A. Pless[g], P. Rankin[k], H. Sagawa[m], T. Sato[f], J. Schneps[n], S.J. Sewell[j], J. Shank[o], A.M. Shapiro[b], J. Shimony[q], R. Sugahara[f], A. Suzuki[f], K. Takahashi[f], K. Tamai[m], S. Tanaka[m], S. Tether[g], D.A. Waide[a], W.D. Walker[c], M. Widgoff[b], C.G. Wilkins[a], S. Wolbers[o‡], C.A. Woods[e#], A. Yamaguchi[m], R.K. Yamamoto[g], S. Yamashita[h], Y. Yoshimura[f], G.P. Yost[o], H. Yuta[m].

a. Birmingham University, Birmingham, England, B15 2TT
b. Brown University, Providence, Rhode Island, 02912
c. Duke University, Durham, North Carolina, 27706
d. Florida State University, Tallahassee, Florida, 32306
e. Imperial College, London, England, SW7 2BZ
f. National Laboratory for High Energy Physics (KEK), Oho-machi, Tsukuba-gun, Ibaraki 305, Japan
g. Massachusetts Institute of Technology, Cambridge, Massachusetts, 02139
h. Nara Womens University, Kita-uoya, Nishi-Machi Nara 630, Japan
i. Oak Ridge National Laboratory, Oak Ridge, Tennessee, 37830
j. Rutherford Appleton Laboratory, Didcot, Oxon., England, OX11 0QX
k. Stanford Linear Accelerator Center, Stanford University, Stanford, California, 94305
l. Technion-Israel Institute of Technology, Haifa 32000, Israel
m. Tohoku University, Sendai 980, Japan
n. Tufts University, Medford, Massachusetts, 02155
o. University of California, Berkeley, California, 94720
p. University of Tel Aviv, Tel Aviv, Israel
q. University of Tennessee, Knoxville, Tennessee, 37996-1200

¶ Present address: University of California, Berkeley, California 94720
◇ Present address, CERN, Geneva, Switzerland
† Present address: American Dade Co., Costa Mesa, CA 92660
‡ Present address: Fermilab, P.O. Box 500, Batavia, IL 60510
# Present address: Rediffusion Simulation, Ltd., Crawley, Sussex, England
♮ Present address: Analytical Sciences Corp., Reading, MA 01867
§ Present address: Santa Cruz Institute of Particle Physics, Santa Cruz, California95064

Submitted to *Physical Review D*

* Work supported in part by the Department of Energy, contract DE-AC03-76SF00515; the Japan-U.S. Co-operative Research Project on High Energy Physics under the Japanese Ministry of Education, Science and Culture; the UK Science and Engineering Research Council; and the U.S. National Science Foundation.

Abstract

The low mass $\omega\pi^0$ enhancement in $\gamma p \rightarrow p\omega\pi^0$ has been of considerable interest in the past due to its suggested vector nature and possible role in the spectroscopy of the rho meson radial recurrences. We have measured the properties of this photoproduced $\omega\pi^0$ system using the SLAC Hybrid Facility. The experimental data consists of 306,785 useable hadronic events for which excellent gamma ray detection is provided by the large lead glass array located behind the bubble chamber. The photon beam had a 52 percent polarization. We have examined in detail the angular distributions of the 274 events from the reaction $\gamma p \rightarrow p\omega\pi^0$. The angular distribution of the production plane relative to the polarization vector shows structure inconsistent with an s-channel helicity conserving process. We have extracted the moments of the decay angular distribution. Our data favors a B(1235) interpretation of the $\omega\pi^0$ state over a vector meson interpretation.

Production and Decay Properties of the $\omega\pi^0$ state at 1250 MeV/c^2 Produced by 20 GeV Polarized Photons on Hydrogen

The radial recurrences of vector mesons are states important to the understanding of the structure of the quark anti-quark interaction. While much detailed data now exists on many of the recurrences of the J/Ψ and the Υ and their transitions[1], knowledge on the ρ recurrences is much more limited. The well established $\rho'(1600)$ is the only reliably detected state. The question of whether there may be another at lower mass is crucial to the understanding of this system. There are some expectations for the first recurrence to appear at about 1200-1300 MeV/c^2.[2] There have been suggestions that this state may be the $\omega\pi^0$ enhancement observed in photoproduction, but the alternate possibility that the enhancement is the B^0(1235) [3] has impeded a conclusive judgement. The first studies of the channel $\gamma p \rightarrow p\omega\pi^0$ [4] revealed a low mass enhancement at $\sim$ 1250 MeV/c^2 in the $\omega\pi^0$ system but were unable to determine the spin parity of the system primarily due to the undetected neutral particles, leaving open the question as to assignment as $\rho'(1250)$ or B^0 meson. They found it was consistent with a diffractively produced vector meson having a peripheral production mechanism and an energy independent cross section. Later, two experiments [5,6] with neutral particle detection concluded that the angular distributions for the $\omega\pi^0$ system required $J^P = 1^-$, although one of them [5] was fighting a substantial

$\gamma p \rightarrow \omega\Delta^+$ background due to its low beam energy. These experiments assumed s-channel helicity conservation (SCHC)[7] in their analysis.

Recently a spin parity analysis[8] of the $\omega\pi^0$ in the above reaction for events produced by photons of 20 to 70 GeV found that the $\omega\pi^0$ enhancement is consistent with predominant 1^+ B(1235) production with a small (20%) $J^P=1^-$ background. They required detection of all four pions in the final state. This severe requirement led to an experimental acceptance of only 0.015 ± 0.005.[9] The proton was identified not by observation but by a measurement of the missing mass of the recoiling baryon system. Their results represent, to date, the most significant investigation of this reaction. We report here new results which complement these earlier measurements. In the present analysis we use events which have a detected and well-measured proton in the bubble chamber and a reconstructed π^0 in the lead glass photon detector. We can then reconstruct the other(undetected) π^0. Since we do have excellent proton detection in the bubble chamber, there is a much higher experimental acceptance than that of reference 8. Furthermore, we have used the high degree of linear polarization of the photon beam in the analysis.

THE EXPERIMENT

This experiment has been described in detail previously.[10] Figure 1 shows the layout. A 20 GeV "monoenergetic" photon beam (produced by Compton backscattering 4.7 eV laser photons from the 30 GeV primary electron beam of the SLAC linear accelerator) is directed

into the SLAC Hybrid Facility (SHF). The energy spectrum of these "monoenergetic" photons is shown in Figure 2. The photons have a $P_\gamma = 0.52$ linear polarization as demonstrated by the elastic ρ^0 decay angular distribution shown in Figure 3 and described in an earlier publication.[11] Most of the events were produced with horizontal polarization (parallel to the magnetic field of the bubble chamber). Twenty-seven per cent of the final sample of 274 events presented below were produced with vertical polarization.

The flash lamps of the SHF 30-inch bubble chamber were triggered by either tracks in the downstream proportional wire chambers (PWC) or energy deposition in the lead glass photon detector.

The most important subsystem of the experiment for the present analysis is the lead glass photon detector which has been described in detail elsewhere.[12] The lead glass array consists of 52 active converter blocks and 152 absorber blocks separated by two planes of one inch wide scintillator fingers. The energy resolution for electrons was measured in a test beam and found to be:

$$\sigma/E = (0.84 + 4.8 \,/\, \sqrt{E})\ \% \qquad \text{(E in GeV)}$$

Excellent π^0 reconstruction was achieved as is illustrated in Figure 4 where a two photon mass spectrum is shown.

DATA ANALYSIS

The 2.4 million pictures taken during this experiment were scanned for hadronic events

and all events found within a fiducial region were fully measured. 306,785 useable events were collected within the 75 cm long fiducial region. The events were associated with the downstream detector measurements with charged tracks being matched to hits in the PWCs. The resulting momentum resolution was

$$\sigma_p/p = ((0.008)^2 + (0.00085p)^2)^{\frac{1}{2}} \qquad \text{(p in GeV/c)}.$$

A crucial ingredient in the analysis of this reaction was the development of a detailed simulation of the SHF and its associated detectors.[13] This Monte Carlo model (PEANUTS) simulates the interaction of all charged and neutral particles in each event with the downstream detectors, simulates the trigger process, for triggered events constructs a raw data record similar to the actual records produced in the experiment, and passes the lead glass pulse height data through the actual reconstruction program which is used to process the real data. In this way all pattern recognition and shower reconstruction from signals in the lead glass blocks are simulated in the Monte Carlo. (See Appendix I for more details.)

This study of the channel $\gamma p \to p\omega\pi^0(\omega \to \pi^+\pi^-\pi^0)$ uses events in which all three charged particles are detected in the bubble chamber and one of the two π^0s is reconstructed from its daughter photons. This results in a clean selection of this channel. Of the 306,785 events measured in the experiment 130,050 were events with three charged tracks emerging from the primary vertex. Events with kinematic fits consistent with the reaction $\gamma p \to p\pi^+\pi^-$ were removed. Only events with a primary vertex within 2.5 millimeters of

the nominal beam center were included in the analysis. Of the remaining events 30,103 had a positive track with momentum under 1.4 GeV/c and ionization and range consistent with a proton. Figure 5 shows the distribution of the mass recoiling from the 3 charged tracks when the photon energy is assumed to be 19.5 GeV. In order to select events consistent with two pi zeros we choose the 21,411 events with this recoiling mass greater than 0.1 $(\mathrm{GeV/c^2})^2$. Figure 6 shows the two photon mass spectrum for these events. The prominent π^0 peak is selected by cutting on the $\gamma\gamma$ mass interval of 120-150 $\mathrm{MeV/c^2}$. This selection misses detected π^0s where the two γs have merged in the lead glass. All of these details, however, are simulated properly by the Monte Carlo program. This yields 6,412 events[14] consistent with the reaction

$$\gamma p \rightarrow p\pi^+\pi^-\pi^0 X.$$

Figure 7 shows the M_X^2 distribution for these events. Selecting $M_X^2 < 0.2$ $(\mathrm{GeV/c^2})^2$, consistent with $\gamma p \rightarrow p\pi^+\pi^-\pi^0\pi^0$, yields 2,405 events. Having associated the X in the above reaction with a π^0 we proceed with a zero constraint calculation of the four pion final state yielding a determination of the incident photon energy. Its distribution is shown in Figure 8. Superimposed on this is the known photon energy distribution from $\gamma p \rightarrow p\pi^+\pi^-$. From this comparison it is clear that the selection of events has produced a photon energy spectrum which closely resembles the known spectrum, confirming the selection process. The difference between the two spectra is reproduced by the Monte

Carlo, being the result of the selection and reconstruction procedure. We further clean this sample by choosing only events with beam photons having reconstructed energies between 15 and 22 GeV, leaving 1833 events.

Figure 9 shows the distribution for the missing π^0 energy. In order to suppress contamination from single π^0 events (such as $\gamma p \rightarrow p\pi^+\pi^-\pi^0$) we select only events with the missing π^0 energy in excess of 1 GeV leaving 1418 events.

The resulting 4π mass distribution is shown in Figure 10. A peak at about 1250 MeV/c^2 is clear, as well as the enhancement in the ρ' (1600) region. Figure 11 shows the $\pi^+\pi^-\pi^0$ mass distribution for the 1418 events. The prominent ω^0 seen is associated with the 1250 MeV/c^2 region as is seen in the lower histogram of Figure 10 where are shown the 415 events with a $\pi^+\pi^-\pi^0$ in the ω^0 region (740-826 MeV/c^2). That the peak in the ω region of the $\pi^+\pi^-\pi^0$ distribution comes both from events where the π^0 is detected and events where it is reconstructed from the missing momentum and energy is shown by the shaded subset of Figure 11. These are the $\pi^+\pi^-\pi^0$ combinations where the π^0 is missing. The ω is seen although it is somewhat broader and weaker than in the total distribution. This characteristic is an understood property of detection and is seen also in the Monte Carlo simulation. Figure 12 presents the t distribution for the 284 events with M($\omega\pi^0$) <1450 MeV/c^2. These events represent a cross section of 0.8 $\pm$ 0.2 μbarns.

THE ANGULAR DISTRIBUTIONS

We have performed a decay angular distribution analysis for the 274 events with $M(\omega\pi^0)$ <1450 MeV/c^2 and $|t_{\gamma\to\omega\pi^0}| < 0.5$ (GeV/c^2)^2. Following the standard convention[15] we describe the decay of the $(\omega\pi^0)$ system into ω and π^0 by the polar (θ) and azimuthal (ϕ) angles of the ω in the helicity rest frame (frame A) of the $(\omega\pi^0)$ system. The orientation of this frame is such that its z axis points in the direction of the $(\omega\pi^0)$ system in the overall c.m. system and its y axis points in the direction of the normal to the production plane. The production plane is defined by the momentum vectors of the $(\omega\pi^0)$ system and the beam in the overall c.m. system. The decay of the ω is described by the spherical angles (β, α) of the normal to the decay plane defined by the $\pi^+\pi^-\pi^0$ in the rest frame of the ω. Two alternative frames were employed. The first, the so called "canonical" frame, is reached from frame A by the Lorentz boost in the direction of the ω, keeping the axes parallel with those of frame A. The (β,α) angles in this frame are denoted β_C and α_C. The second frame, the so called "helicity" frame, has its z axis pointing in the direction of the ω in the frame A and its y-axis given by the vector products of the ω direction and the z axis of frame A. The (β,α) angles in this frame are denoted β_H and α_H.[16]

We have also examined the angular distributions of $\psi = \phi - \Phi$ and $\psi' = \alpha_C - \Phi$, where Φ is the angle between the polarization vector of the photon and the production

plane, as these are important parameters in the analysis of meson production by polarized photons[17].

Figures 13 show the distributions of these angles for our data. The acceptance of our detector has been modeled as previously described and discussed in Appendix I. The acceptance of the photon detector has a strong effect on the observed distribution with approximately 20 per cent of the produced events selected by the procedure outlined above (see Table I). Note that this represents an order of magnitude increase over the acceptance of reference 8. Our acceptances are rather uniform in the angular distribution (see Appendix I). Many comparisons have been made between the data and the acceptance Monte Carlo. Figure 14 shows, for example, the separation between gammas at the lead glass detector for the 274 events with an expected curve from the Monte Carlo superimposed. The agreement is excellent. Figure 15 shows the calculated distribution of acceptance for the 274 observed events compared with the expected acceptance curve for accepted events. Again the Monte Carlo represents the data reasonably well.

The most general form for the Φ distribution is

$$I(\Phi) = \frac{1}{2\pi}(1 + a\ cos(2\Phi) + b\ sin(2\Phi))$$

It follows from parity conservation [17] that b = 0. Imposing this constraint and fitting the distribution of Figure 16 for a we obtain a = -0.36 ± 0.08 with a χ^2 of 24 (C.L.=0.20). This fit is shown superimposed on Figure 16. This can be compared to the χ^2 for a

flat distribution of 45 (C.L.=0.001) and represents a very significant deviation from the necessary condition of s-channel helicity conservation, that $I(\Phi) = constant.$ [17] This significant indication of non-conservation of s-channel helicity supports the conclusions of reference 8.

We have adopted the parametrization of reference 8 to represent our angular distributions. They parametrized the distributions following reference 15:

$$\frac{dN}{d\Omega\ d\Omega_H\ d\Phi} = \frac{N}{2\pi}(W_0(\Omega,\Omega_H) - PW_1(\Omega,\Omega_H)cos(2\Phi) - PW_2(\Omega,\Omega_H)sin(2\Phi))$$

$$W_k(\Omega,\Omega_H) = \sum_\alpha H^{k\pm}_s(\alpha)H^{\pm}_\alpha(\Omega,\Omega_H)/C_\alpha \qquad \alpha = lmLM$$

where the 25 orthogonal functions[15] $H^{\pm}_{lmLM}(\Omega,\Omega_H)$ (given in Table 1 of reference 8[18]) are related to the Wigner D functions (see Appendix II).

Note that reference 8 determined the moments $H^{0\pm}_s(\alpha)$ but did not succeed in obtaining measurements of $PH^{1\pm}_s(\alpha)$ and $PH^{2\pm}_s(\alpha)$. With our higher degree of beam polarization we have been able to find all three sets of moments, although our smaller data sample yields somewhat larger experimental errors on $H^{0\pm}_s(\alpha)$. As described in Appendix II, we have obtained the acceptance corrected values shown in Table II. Having obtained these we show as solid curves on Figure 13 the expected distributions after acceptance. The χ^2 for the 8 histograms is 156 for 159 degrees of freedom. We have also used the Omega Photon Collaboration measured values for $H^{0\pm}_s(\alpha)$ and calculated the expected distributions corrected for our acceptance. These curves are shown superimposed on our

data in Figure 13 as the dashed curves. Again the agreement is very good, having a χ^2 of 132 for the 119 degrees of freedom. Note that no comparison has been made here for the ψ and ψ' distributions since the Omega Photon Collaboration does not provide the polarization moments.

We did not attempt to perform an analysis using all these moments because of the large number of parameters involved, in particular those describing details of the production of various states (i.e. the ρ matrix) and their interferences. However, the angular distribution of $cos\beta_H$ is of particular interest because it depends only on the decay properties of a given spin-parity state and not on the details of its production. In terms of moments it is given by

$$\frac{dN}{d\ cos\beta_H} = \frac{N}{2}(1 + 5H_s^{0+}(2000)d_{00}^2)$$

$$d_{00}^2 = \frac{1}{2}(3cos^2\beta_H - 1)$$

which reduces to

$$\frac{dN}{d\ cos\beta_H} = \frac{3N}{2}(|F_1|^2 sin^2\beta_H + |F_0|^2 cos^2\beta_H)$$

where F_λ is the conventional decay amplitude[15] for an ω of helicity λ. Table III shows the value for $|F_1|^2$ extracted from our measurement of the moment $H_s^{0+}(2000)$. The table makes a comparison with the expectations for the production of pure 0^-, 1^-, and B(1235). From this comparison one sees that the best agreement comes from the B(1235). A mixture of 1^- with a 0^- background, however, can also be made to agree with the data.

The experimental value for $H_s^{0+}(2000)$ would require a mixture of 77 $\pm$ 6 percent 1^- and 23 $\pm$ 6 percent 0^-. Figure 10 for the $\omega\pi^0$ mass suggests that such a large non-resonant background is unlikely. On the otherhand, only 13 percent 0^- background is required to make the 1^- case as close to agreement with the data as that of the B(1235). This cannot be ruled out. Therefore the situation is ambiguous with a slight preference for the B(1235).

CONCLUSIONS

We have examined in detail the decay angular distributions for the $\omega\pi^0$ system in the reaction $\gamma p \rightarrow p\omega\pi^0$. The angular distribution of the production plane relative to the photon polarization vector shows structure inconsistent with an s-channel helicity conserving process. We have compared our data to the parameterization obtained by the Omega Photon Collaboration of the same process. Our measurement is complementary in a number of aspects. First our acceptance is about an order of magnitude greater. Second we detect recoiling protons in the bubble chamber. Third we make use of our high degree of linear polarization to measure the polarization-dependent moments. Our decay angular distributions agree with the measurement of the Omega Photon Collaboration[8]. From the $cos\beta_H$ distribution we conclude that our data marginally favors a B(1235) interpretation of the $\omega\pi^0$ state over a vector meson.

ACKNOWLEDGEMENTS

We benefited during the preparation of this paper from discussions with Professors F. Gilman and B.F.L. Ward.

REFERENCES

1. See for example Particle Data Group, Physics Letters 170B, 1 (1986).

2. H.J.Schnitzer, Phys. Rev. 18, 3482 (1978).

3. The $B^0(1235)$ is b1(1235) in the convention of the Particle Data Group.

4. R. Anderson et al, Phys. Rev. D1, 27 (1970); J. Ballam et al, Nucl. Phys. B76, 375 (1974).

5. D.P. Barber et al, Z. Phys. C4, 169 (1980).

6. D. Aston et al, Phys. Lett. 92B, 211 (1980).

7. F.J. Gilman, J. Pumplin, A. Schwimmer, and L. Stodolsky, Phys. Lett. B31, 387, (1970).

8. M. Atkinson et al, Nucl Phys. B243, 1 (1984).

9. R.H. McClatchey, University of Sheffield thesis, HEP/T/92, November, 1981.

10. K. Abe et al, Phys. Rev. D30, 1 (1984).

11. K. Abe et al, Phys. Rev. Lett. 53, 751 (1984).

12. J.E. Brau et al, Nucl. Inst. and Methods 196, 403 (1982).

13. J.E. Brau, SLAC BC75 Note 41, February 27, 1984, internal documentation.

14. Some events are selected by each cut in this analysis more than once. When this occurs, multiple entries are included in the histograms.

15. S.U. Chung, CERN Yellow Report 71-8 (1971). S.U. Chung et al, Phys. Rev. D11, 2426 (1975).

16. Note that β_H and α_H of this paper are identical to θ_H and ϕ_H of reference 8.

17. K. Schilling, P. Seyboth, and G. Wolf, Nucl. Phys. B15, 397 (1970).

18. We have found two errors in Table 1 of reference 8. Equation 4 should have a coefficient of $\frac{\sqrt{6}}{4}$ rather than $\sqrt{\frac{6}{4}}$. Equation 8 should have a coefficient of $\frac{\sqrt{6}}{8}$ rather than $\sqrt{\frac{6}{8}}$.

LIST OF TABLES

TABLE I
Selection efficiencies

selection	efficiency
triggered	0.99
visible proton	0.95
$M_X^2 > 0.1$	0.94
at least 2γ	0.85
$2\gamma{=}\pi^0$	0.46
$M_X^2 < 0.2 \text{and} 15 < E_\gamma < 22$	0.74
$M_{\omega\pi^0} < 1450 MeV/c^2$	0.75
Total efficiency	0.19

TABLE II

$\pm\ lmLM(\alpha)$	$H^{0\pm}_{s}(\alpha)$	$PH^{1\pm}_{s}(\alpha)$	$PH^{2\pm}_{s}(\alpha)$
+ 0000	1.000 ± 0.000	0.231 ± 0.126	-0.085 ± 0.125
+ 0020	0.034 ± 0.037	0.027 ± 0.063	0.027 ± 0.063
+ 0021	0.048 ± 0.022	0.007 ± 0.034	-0.005 ± 0.032
+ 0022	0.003 ± 0.018	-0.026 ± 0.025	0.006 ± 0.026
+ 2000	-0.060 ± 0.035	-0.074 ± 0.050	-0.040 ± 0.052
+ 2020	0.023 ± 0.018	0.015 ± 0.024	-0.008 ± 0.026
+ 2021	-0.005 ± 0.010	-0.013 ± 0.015	-0.005 ± 0.014
+ 2022	0.000 ± 0.007	-0.006 ± 0.010	0.006 ± 0.011
+ 2120	-0.005 ± 0.008	0.008 ± 0.012	0.013 ± 0.012
+ 2121	-0.006 ± 0.007	-0.007 ± 0.010	-0.005 ± 0.010
+ 2122	-0.006 ± 0.005	0.013 ± 0.008	0.001 ± 0.007
+ 2220	0.009 ± 0.008	0.022 ± 0.012	-0.005 ± 0.012
+ 2221	-0.009 ± 0.006	-0.010 ± 0.009	-0.002 ± 0.009
+ 2222	-0.015 ± 0.008	0.027 ± 0.012	-0.002 ± 0.012
+ 2111	0.010 ± 0.010	0.010 ± 0.014	-0.007 ± 0.013
− 0010	0.209 ± 0.046	0.137 ± 0.067	-0.068 ± 0.065
− 0011	0.067 ± 0.025	0.099 ± 0.035	0.014 ± 0.034
− 2110	-0.026 ± 0.009	0.006 ± 0.013	-0.002 ± 0.013
− 2111	0.002 ± 0.009	0.006 ± 0.014	-0.008 ± 0.013
− 2121	0.009 ± 0.007	-0.000 ± 0.010	-0.006 ± 0.010
− 2122	0.004 ± 0.005	0.004 ± 0.007	-0.010 ± 0.007
− 2221	-0.007 ± 0.006	-0.002 ± 0.009	0.001 ± 0.009
− 2222	-0.008 ± 0.008	0.020 ± 0.012	-0.001 ± 0.011
− 2010	-0.034 ± 0.021	0.014 ± 0.029	-0.035 ± 0.030
− 2011	-0.007 ± 0.010	-0.014 ± 0.014	-0.004 ± 0.015

TABLE III

	$H_s^{0\pm}(2000)$	$\lvert F_1\rvert^2$
data	-0.060 ± 0.035	0.383 ± 0.029
0^-	0.400	0.000
1^-	-0.200	0.500
B(1235) $(\frac{d}{s} = 0.26 \pm 0.035)$	-0.124 ± 0.014	0.437 ± 0.012

LIST OF FIGURES

1. The SLAC Hybrid Facility with bubble chamber, proportional wire chambers, Cherenkov counters, lead-glass columns, and beam-stop counter.

2. The photon-energy spectrum measured by the pair spectrometer in front of the bubble chamber.

3. $dN/d\psi$ for $\gamma p \to \rho(770)p$.

4. Inclusive $\gamma - \gamma$ mass spectrum for the lead glass columns after selecting pairs with total energy greater than 4 GeV.

5. Distribution of mass recoiling from the three charged tracks in $\gamma p \to p\pi^+\pi^-$

6. The $\gamma - \gamma$ mass spectrum for events with a mass in Figure 5 greater than 0.1 $(GeV/c^2)^2$.

7. The M_X^2 distribution for $\gamma p \to p\pi^+\pi^-\pi^0 X$.

8. Beam energy distribution for the reaction $\gamma p \to p\pi^+\pi^-\pi^0(\pi^0)$. The solid curve is the beam spectrum from $\gamma p \to p\pi^+\pi^-$.

9. Missing π^0 energy distribution.

10. Four π mass distribution. The shaded histogram is after ω selection.

11. $\pi^+\pi^-\pi^0$ mass distribution from the reaction $\gamma p \to p\pi^+\pi^-\pi^0(\pi^0)$. The shaded histogram is the distribution for the combinations with missing π^0s.

12. $t_{\gamma \to 4\pi}$ distribution.

13. The angular distributions. The solid curves are the results of the moments analysis from the present experiment and the dashed curves are the results from reference 8. Both curves show the expected distribution for this experiment after acceptance.

14. Separation between gammas at the lead glass detector for the 274 events of the type $\gamma p \to p\pi^+\pi^-\pi^0(\pi^0)$ used in this analysis. The curve is the expected distribution from the PEANUTS Monte Carlo.

15. Calculated acceptance distribution for the 274 events used in the analysis. The curve is the expected distribution from the PEANUTS Monte Carlo.

16. Φ distribution with fit as described in text.

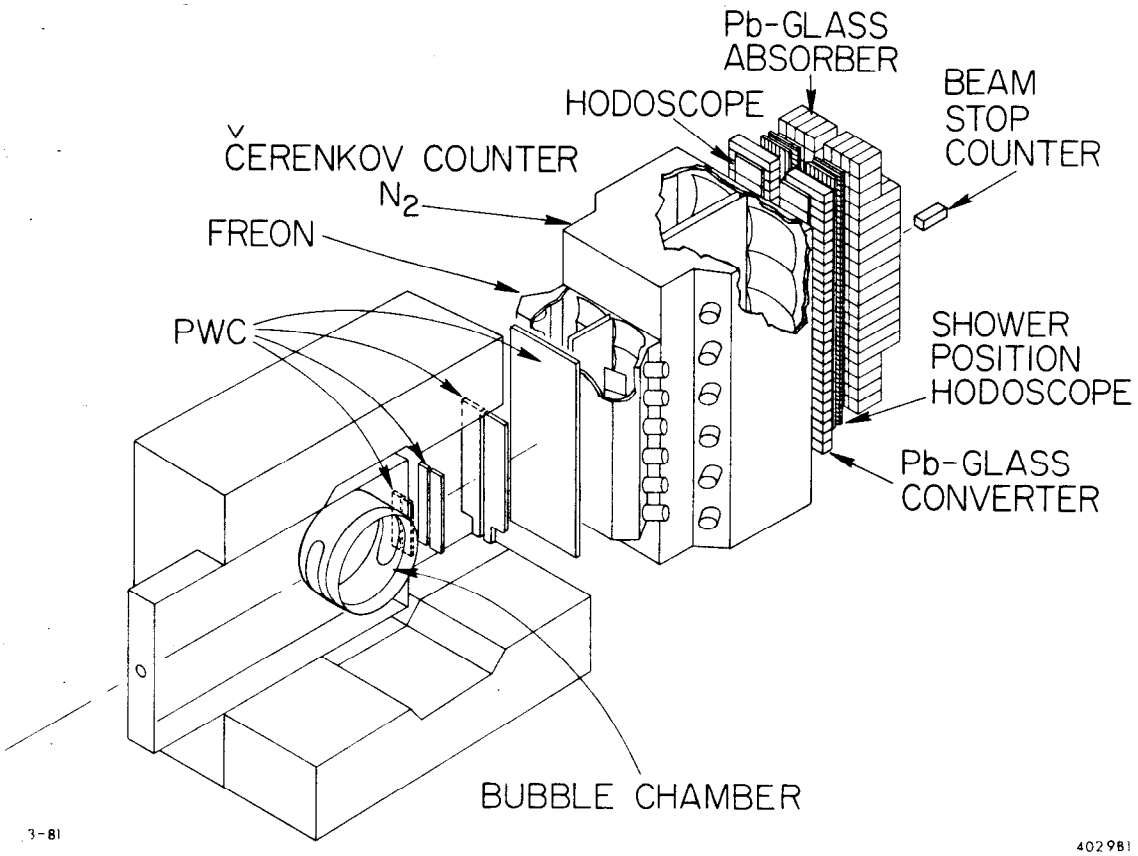
Pb-GLASS
ABSORBER
HODOSCOPE
BEAM
STOP
COUNTER
CERENKOV COUNTER
N_2
FREON
PWC
SHOWER
POSITION
HODOSCOPE
Pb-GLASS
CONVERTER
BUBBLE CHAMBER
3-81
402981

Figure 1

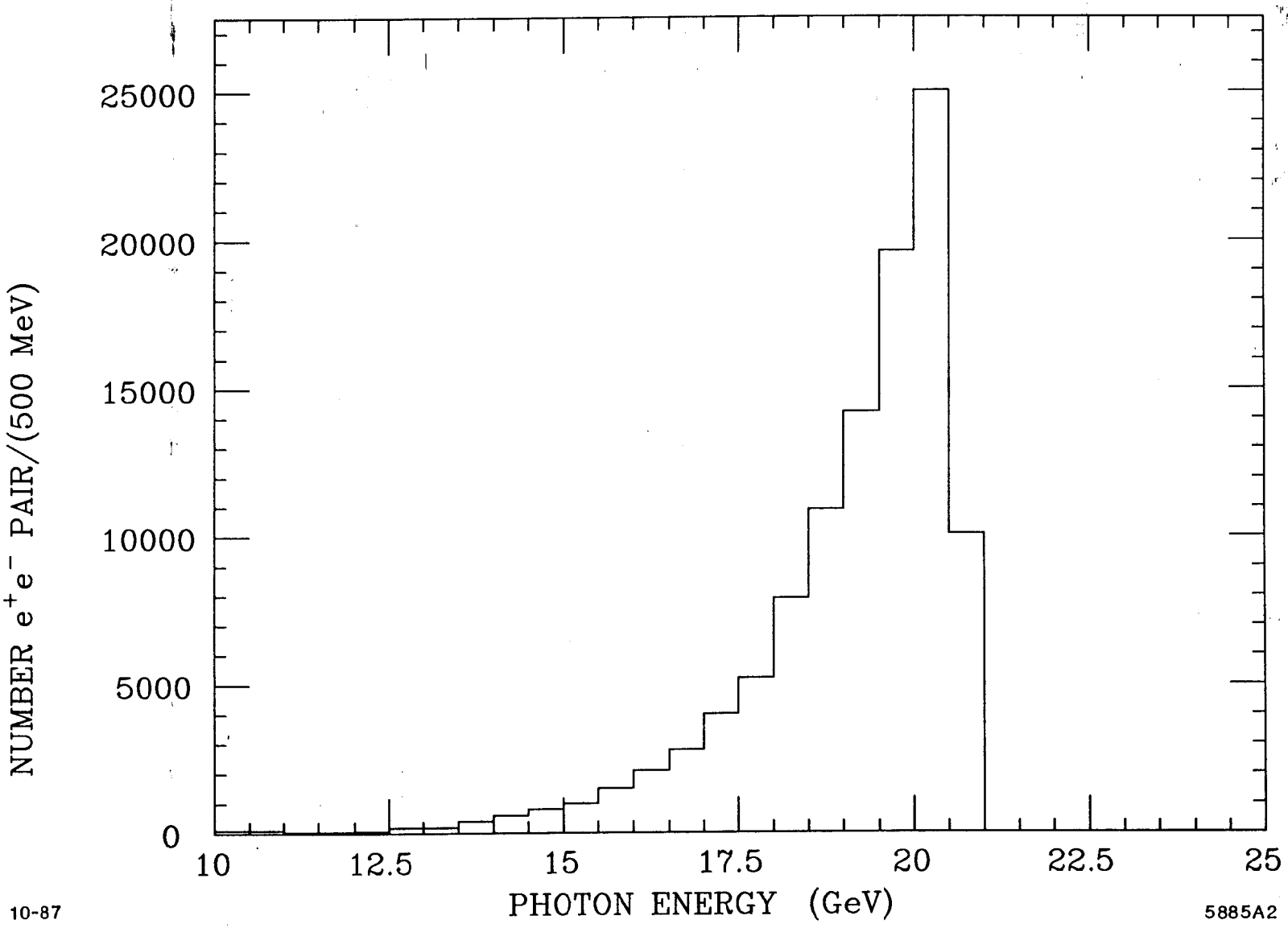
25000
20000
15000
10000
5000
0
NUMBER e^+e^- PAIR/(500 MeV)
10
12.5
15
17.5
20
22.5
25
PHOTON ENERGY (GeV)
10-87
5885A2

Figure 2

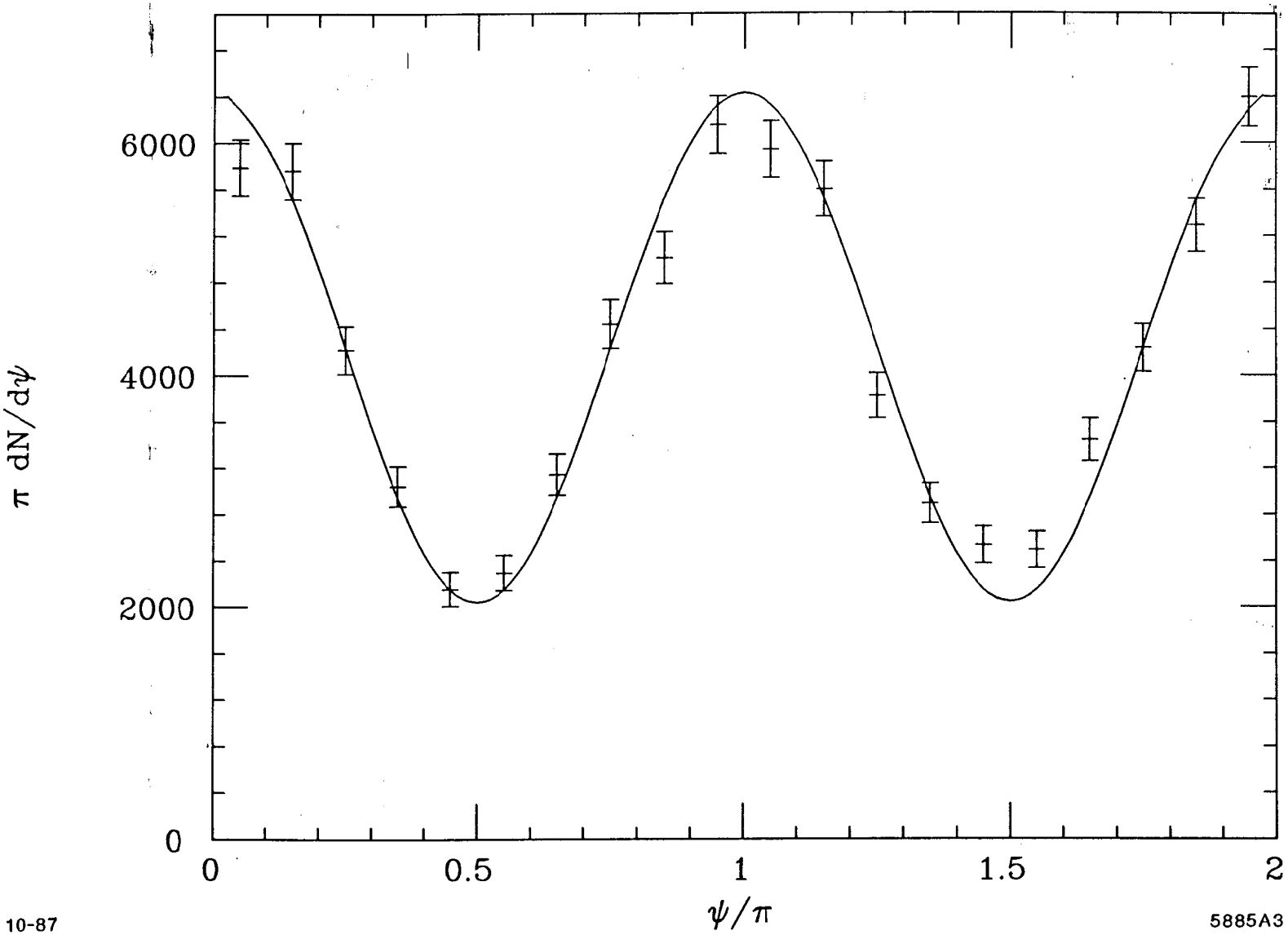

Figure 3

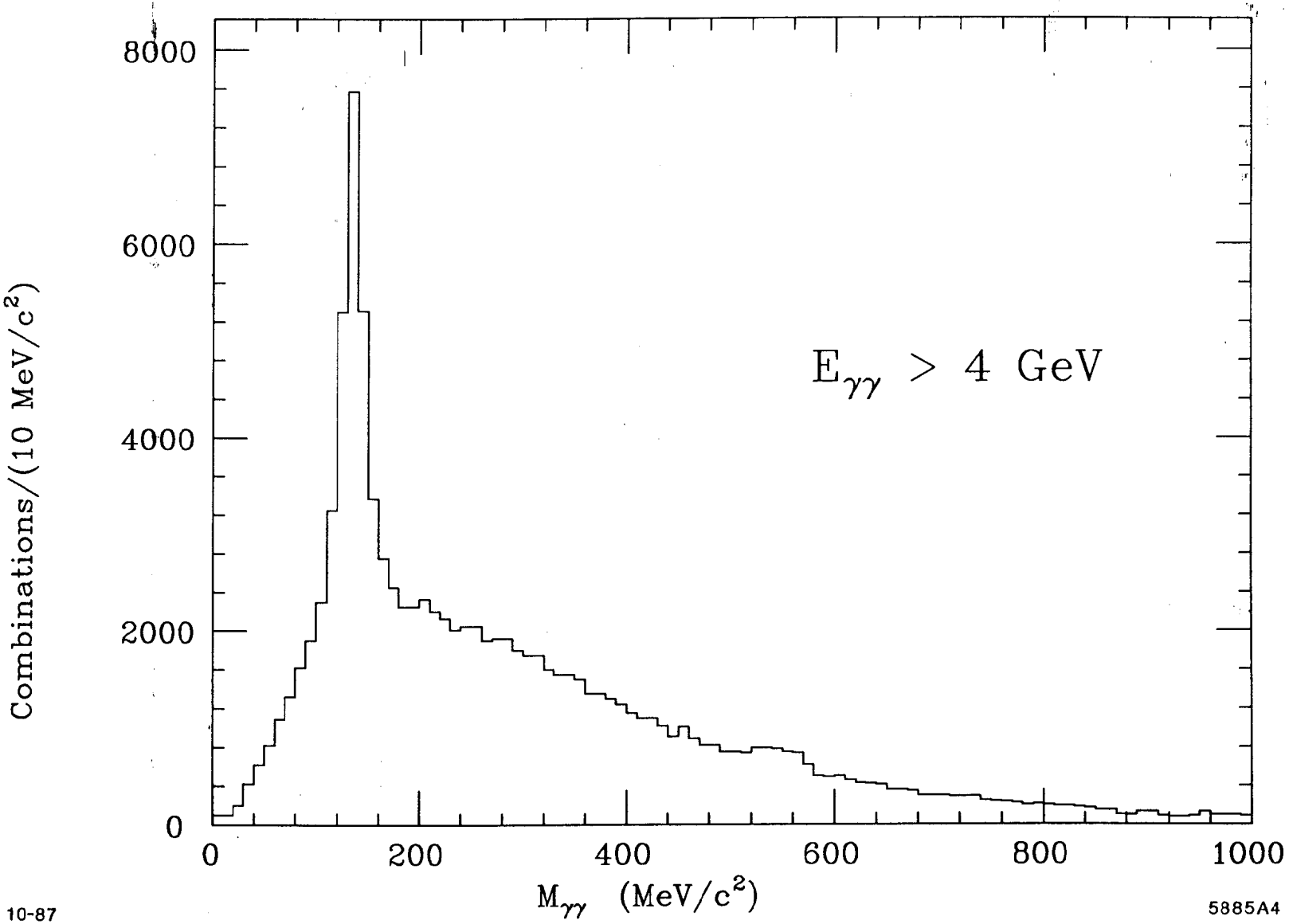
8000
6000
4000
2000
0
0
200
400
600
800
1000
Combinations/(10 MeV/c^2)
$M_{\gamma\gamma}$ (MeV/c^2)
$E_{\gamma\gamma} > 4$ GeV
10-87
5885A4

Figure 4

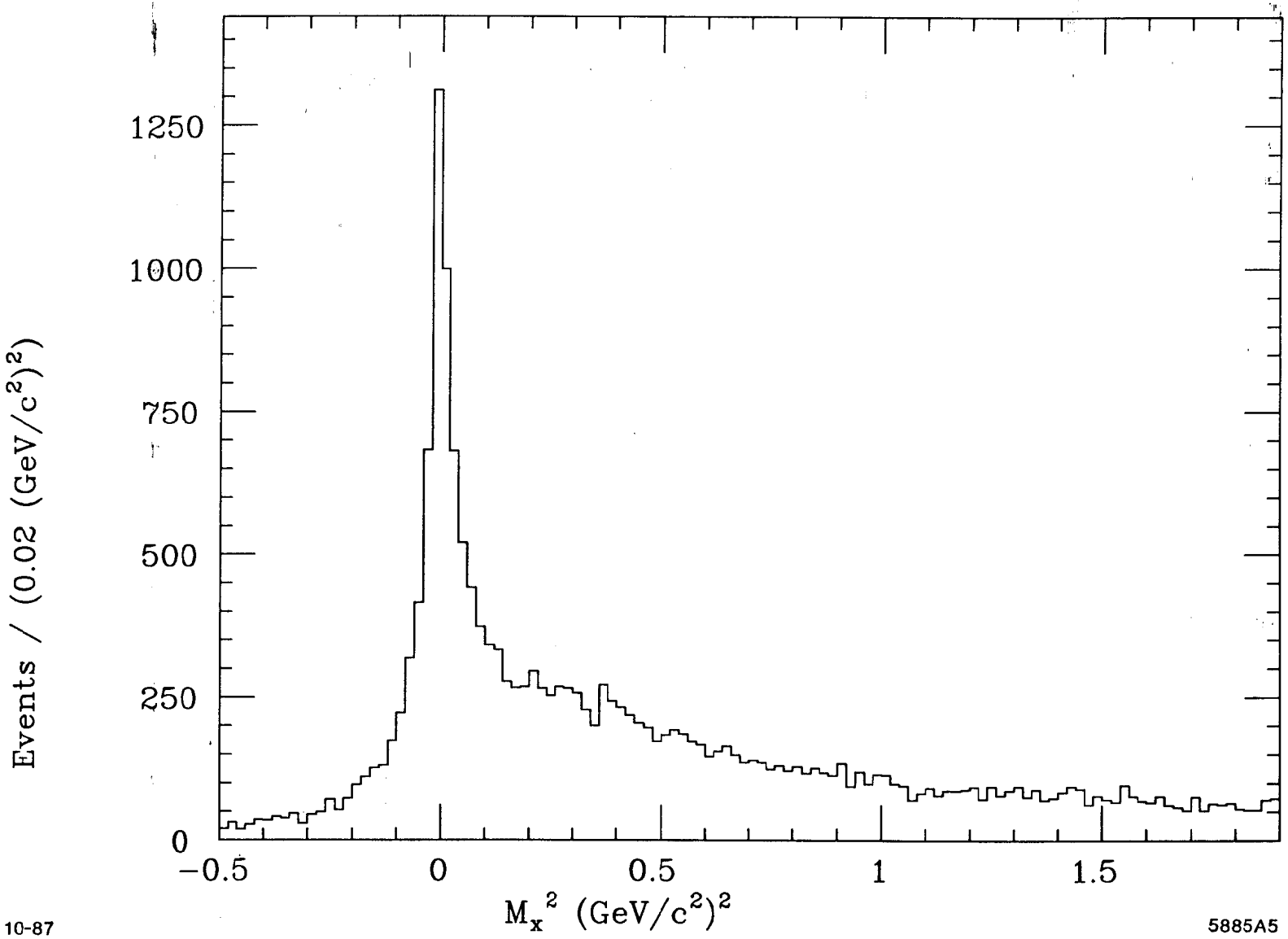
1250
1000
750
500
250
0
−0.5
0
0.5
1
1.5
Events / (0.02 (GeV/c²)²)
M_x² (GeV/c²)²
10-87
5885A5

Figure 5

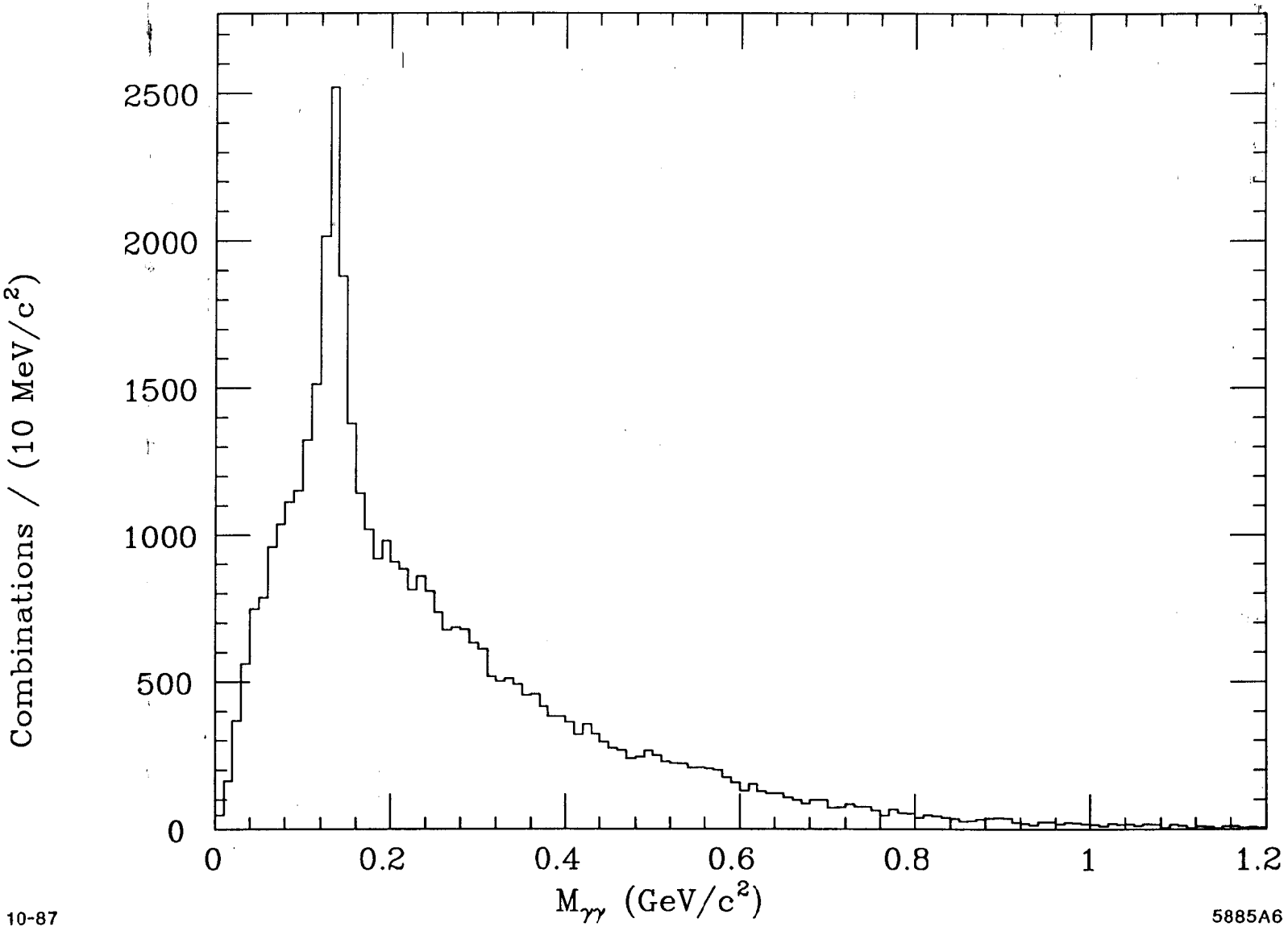
Combinations / (10 MeV/c²)
2500
2000
1500
1000
500
0
0
0.2
0.4
0.6
0.8
1
1.2
M$_{\gamma\gamma}$ (GeV/c²)
10-87
5885A6

Figure 6

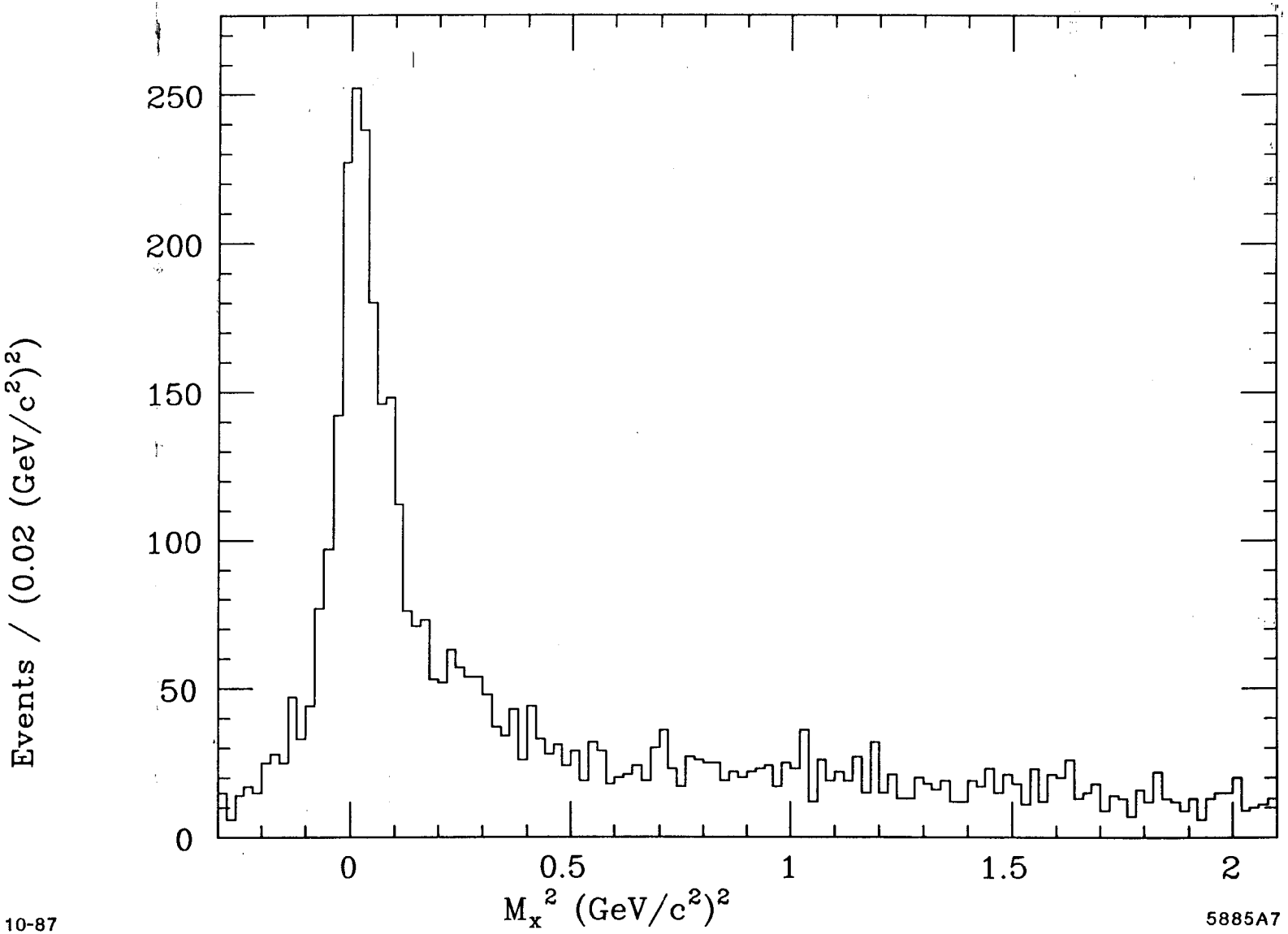
Events / (0.02 (GeV/c^2)^2)
250
200
150
100
50
0
0
0.5
1
1.5
2
M_x^2 (GeV/c^2)^2
10-87
5885A7

Figure 7

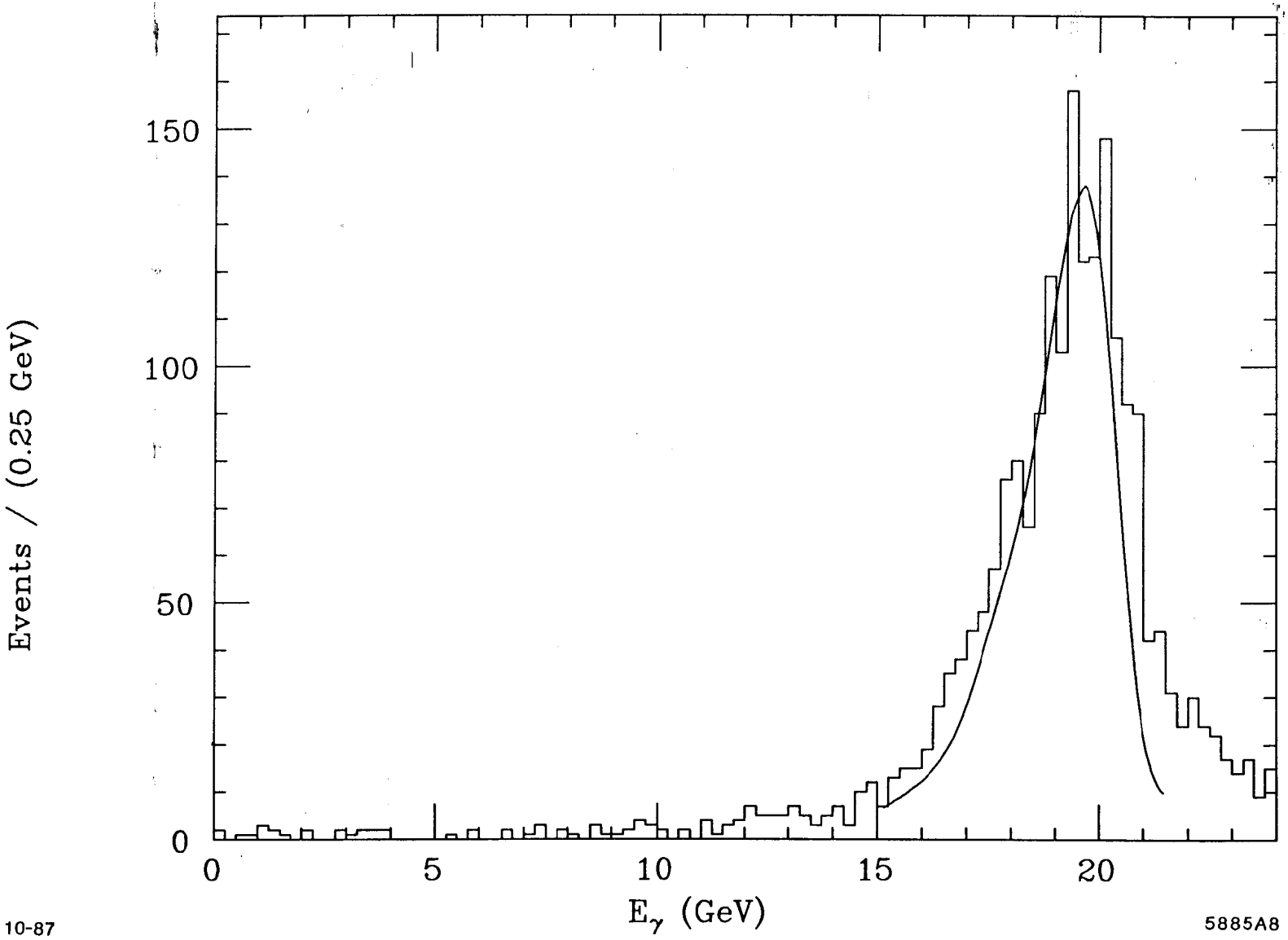

Figure 8

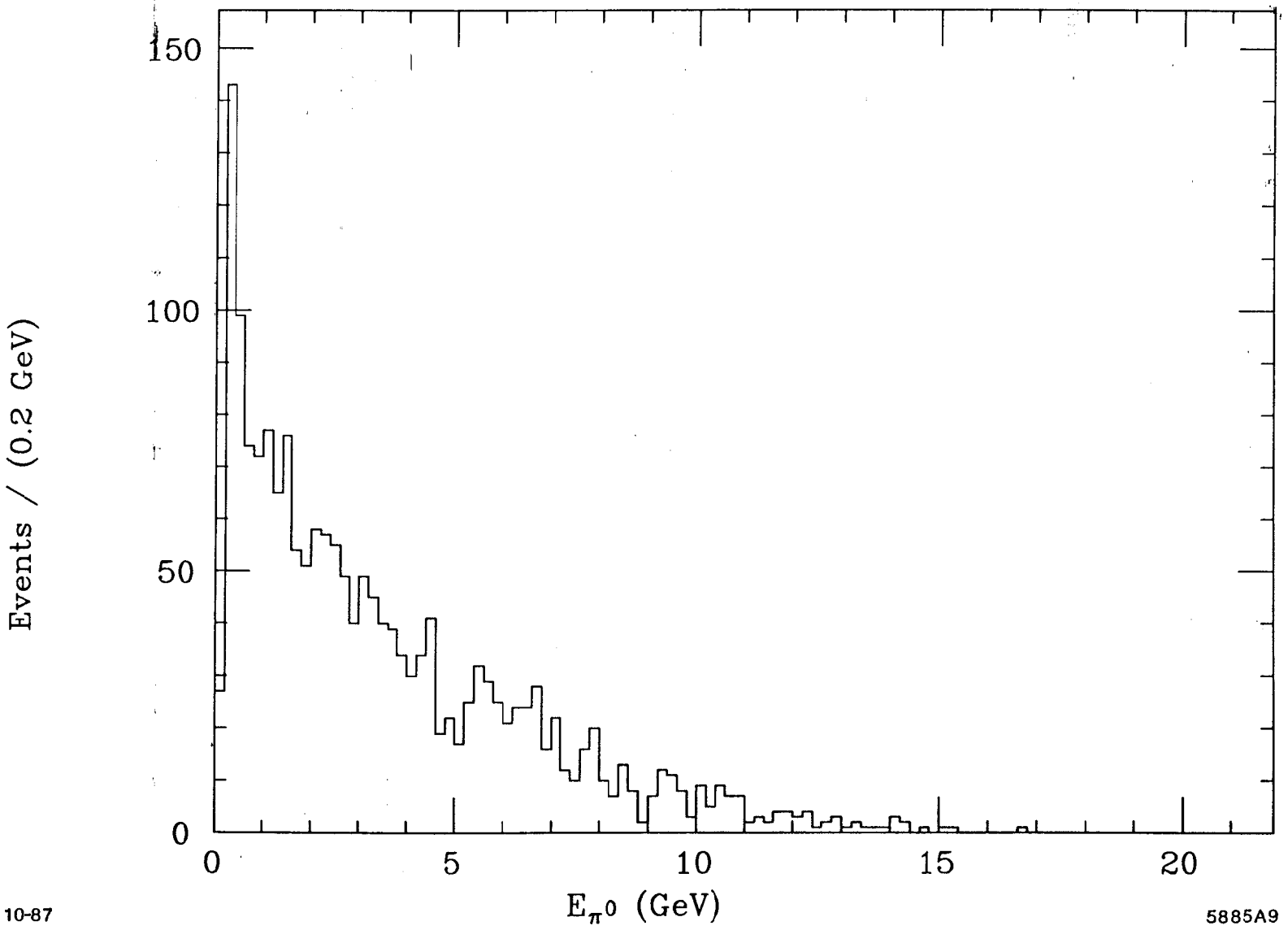

Figure 9

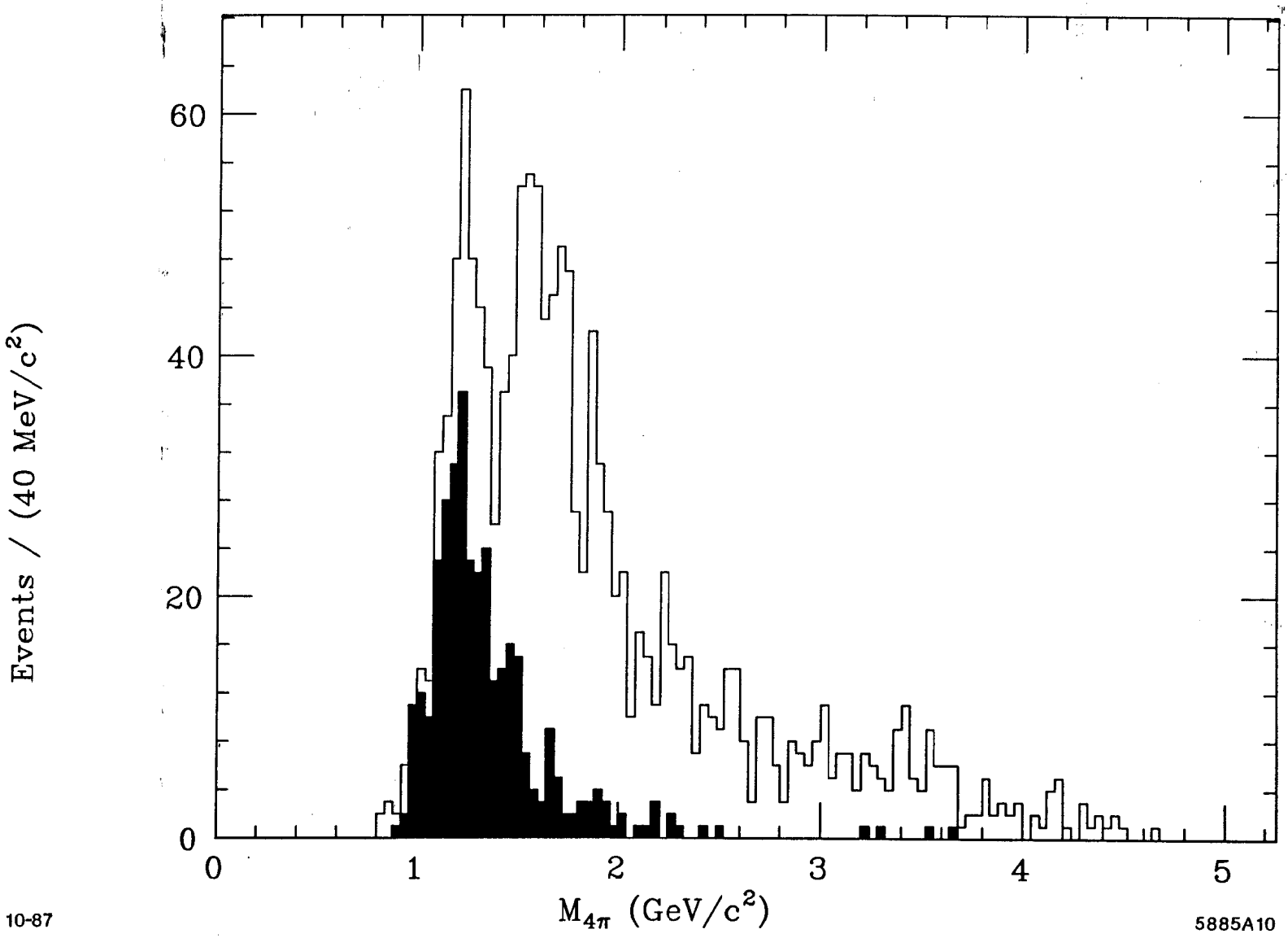

Figure 10

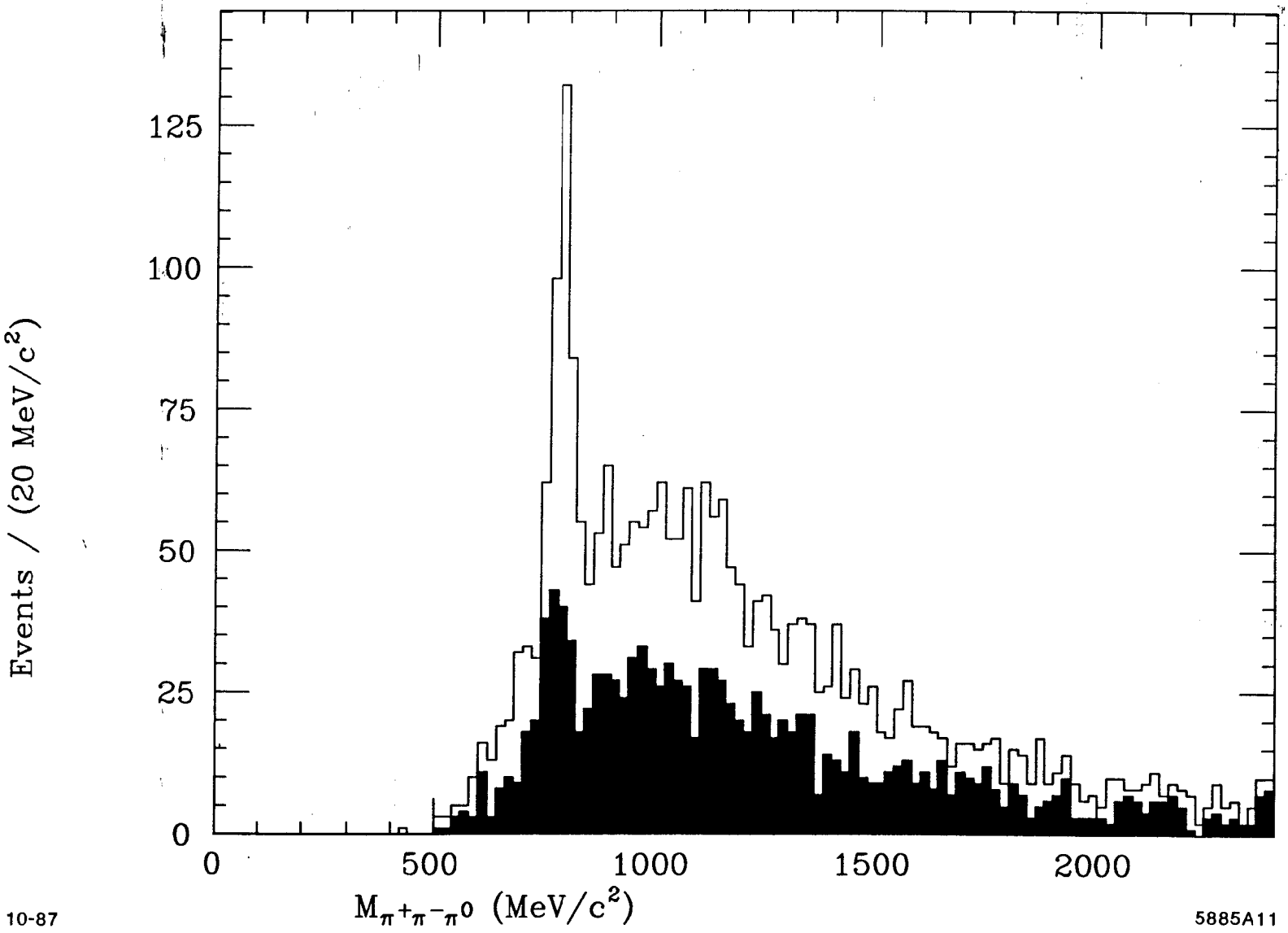
125
100
75
50
25
0
0
500
1000
1500
2000
Events / (20 MeV/c^2)
$M_{\pi^+\pi^-\pi^0}$ (MeV/c^2)
10-87
5885A11

Figure 11

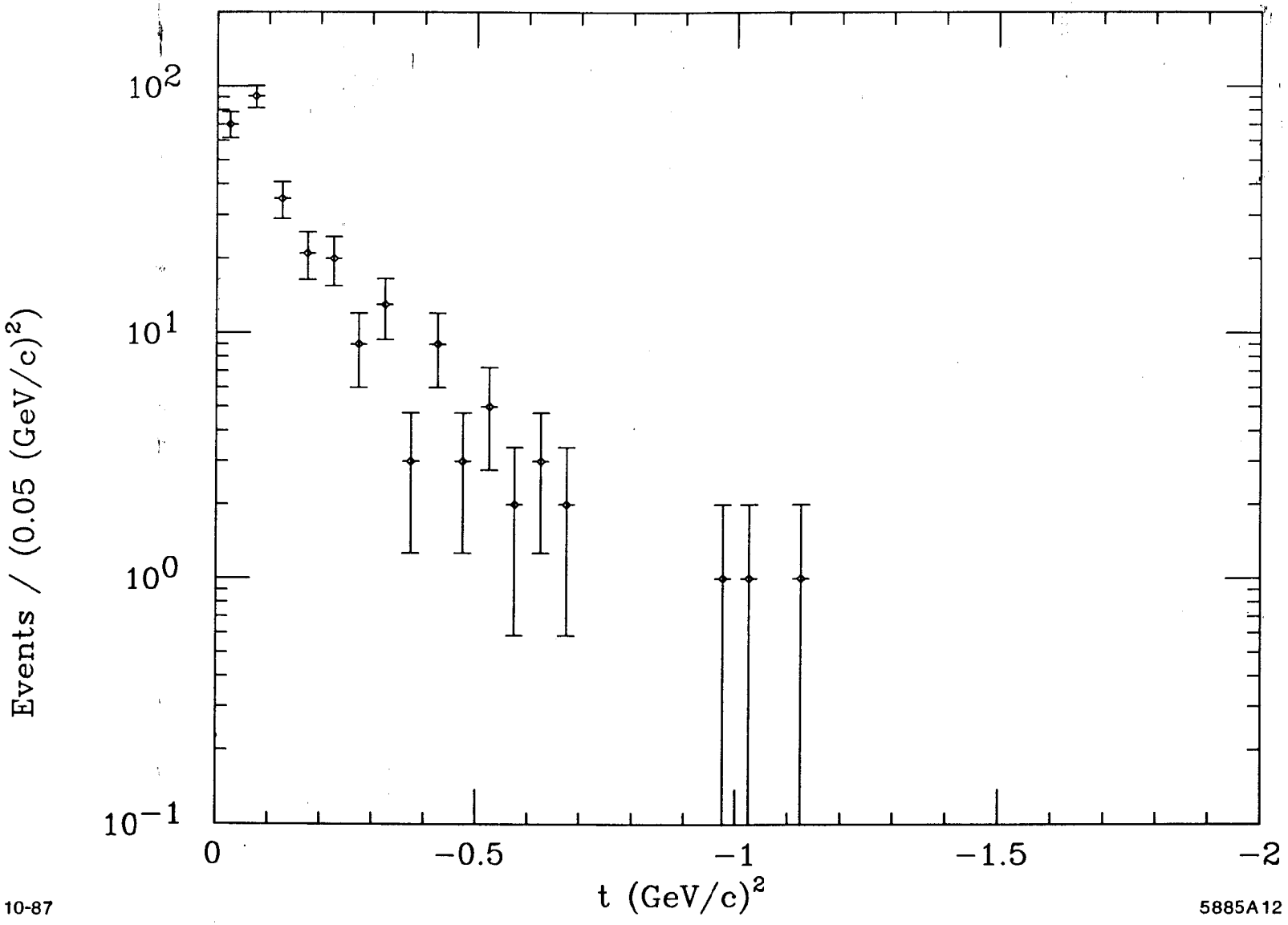
10^2
10^1
10^0
10^{-1}
Events / (0.05 (GeV/c)^2)
0
−0.5
−1
−1.5
−2
t (GeV/c)^2
10-87
5885A12

Figure 12

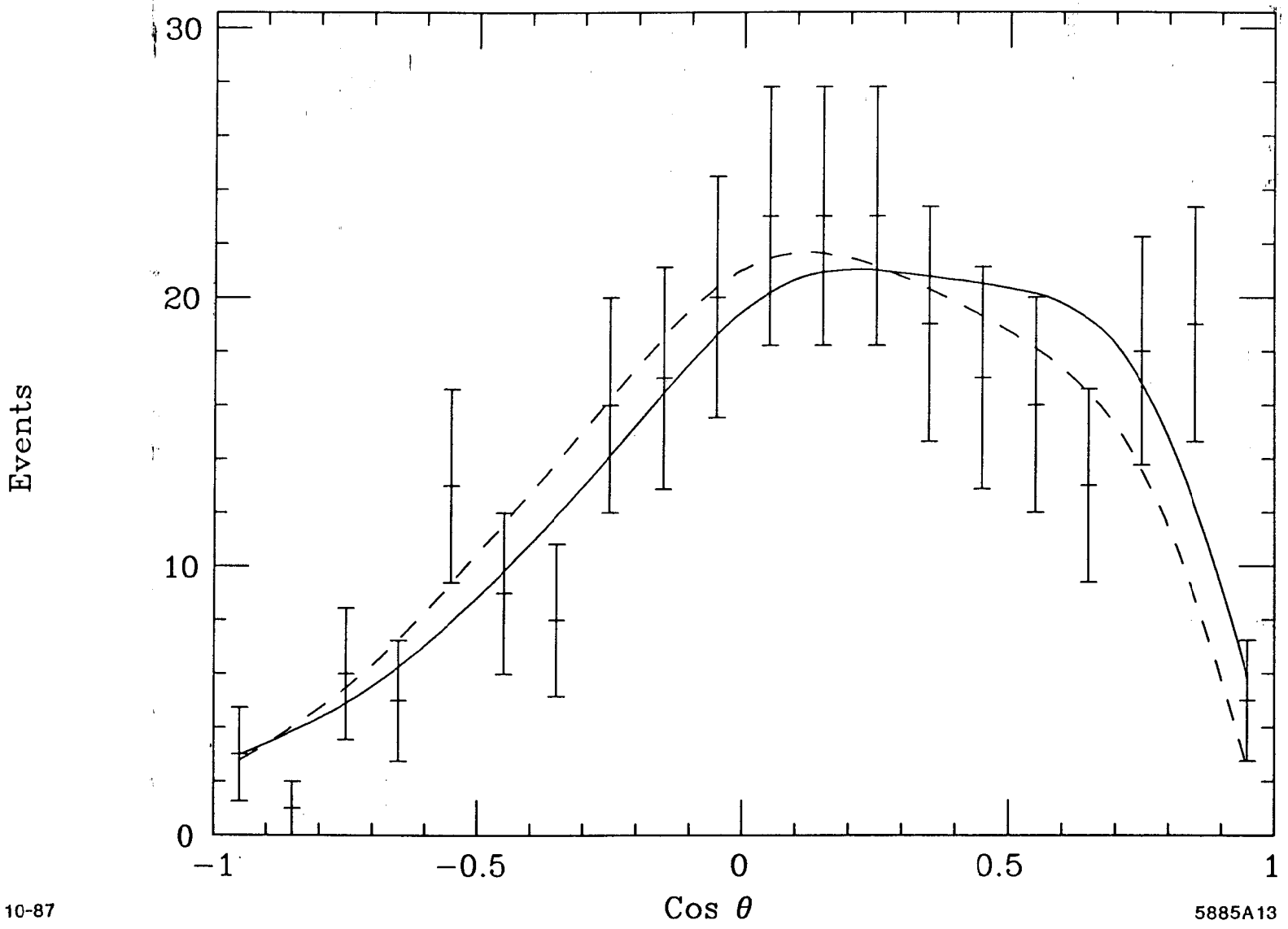

Figure 13a

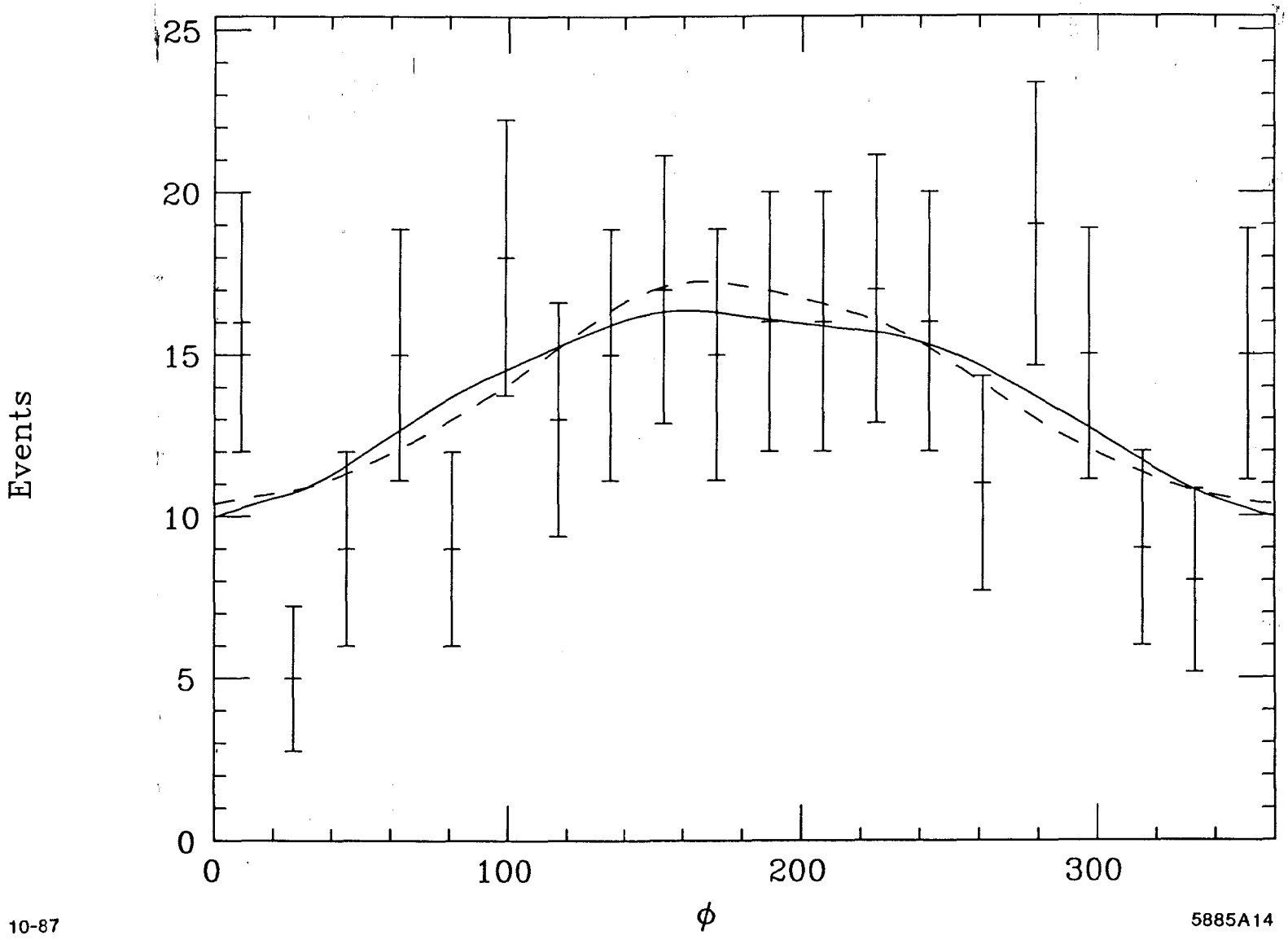

Figure 13b

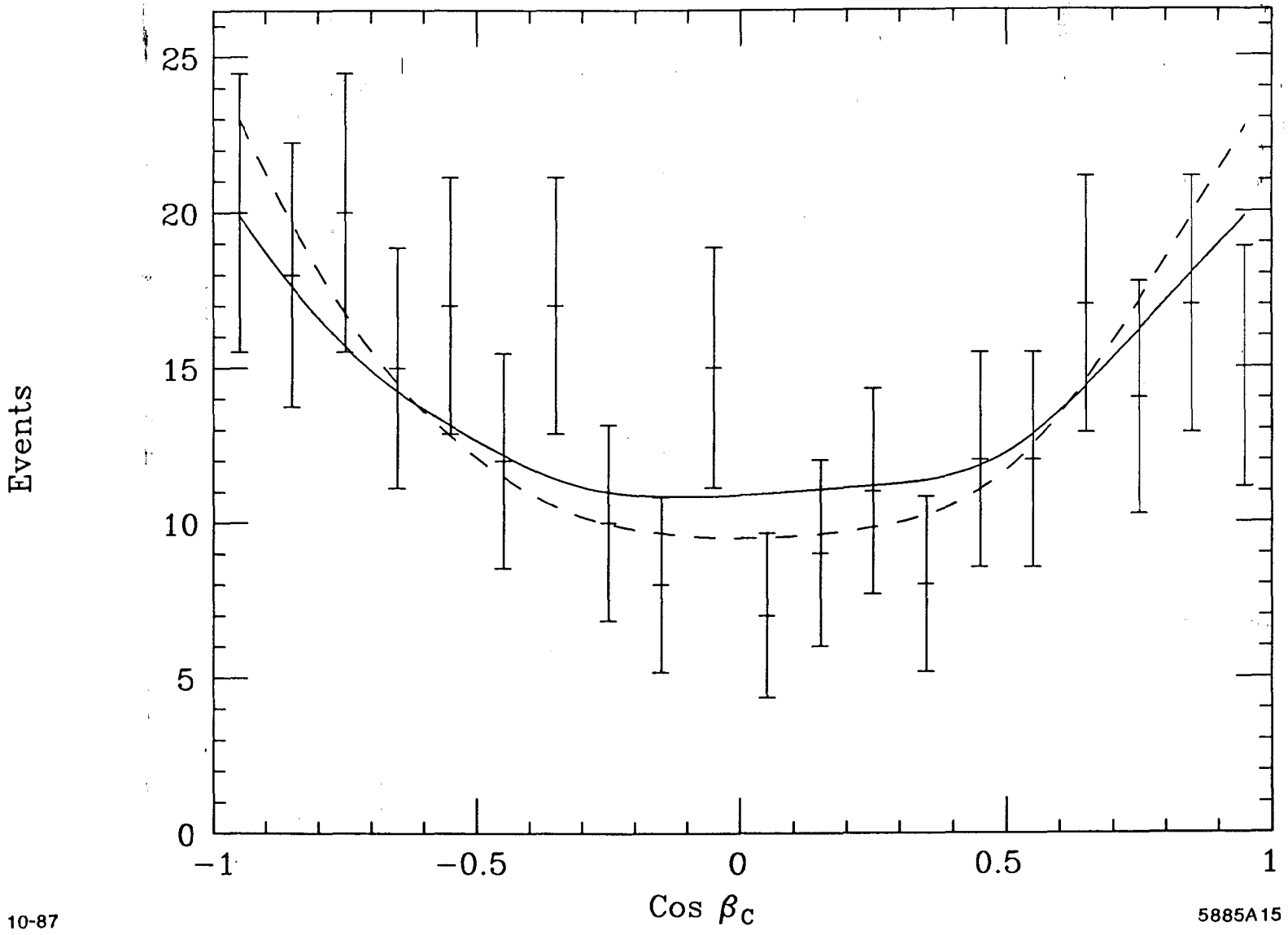

Figure 13c

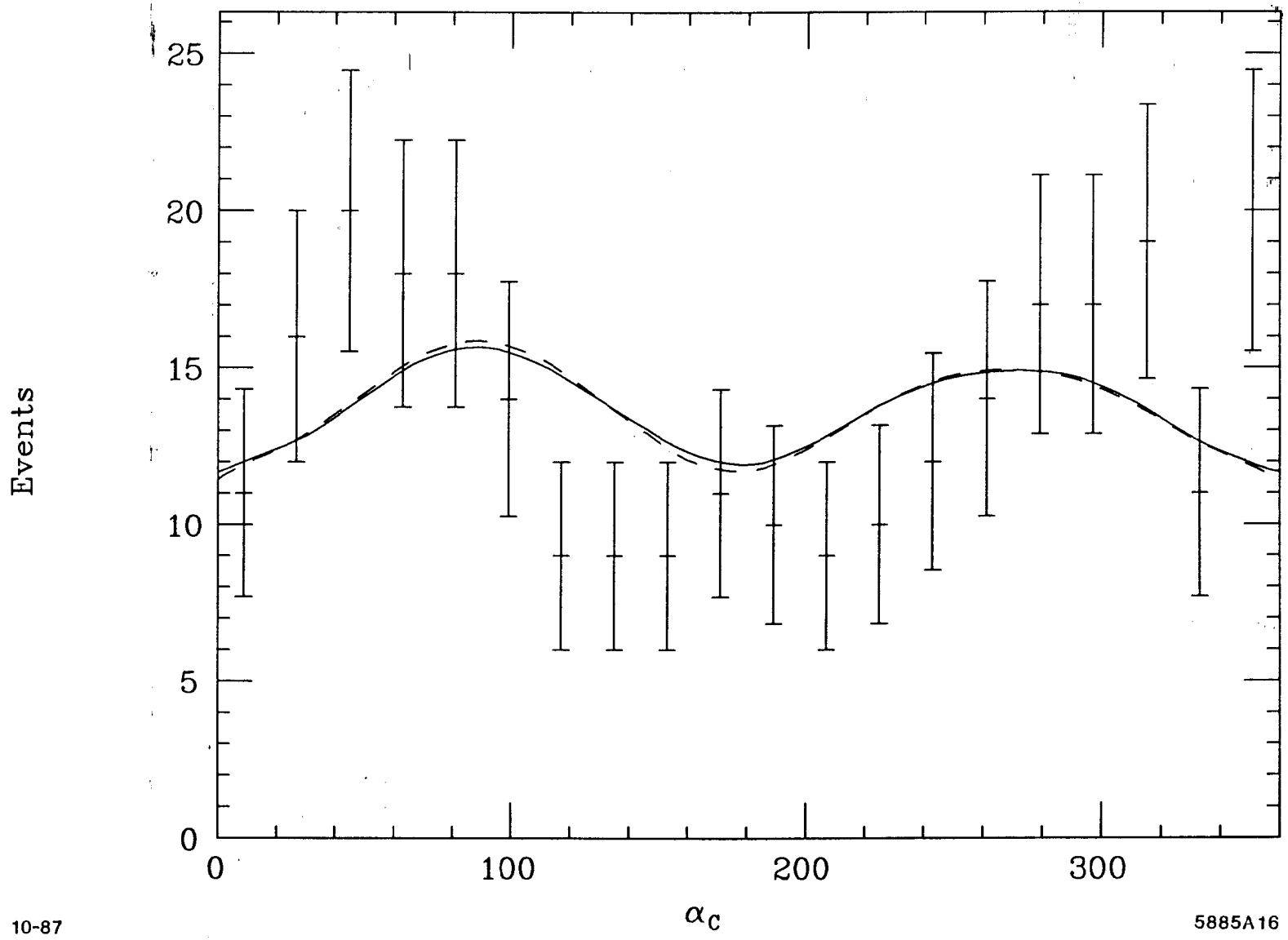

Figure 13d

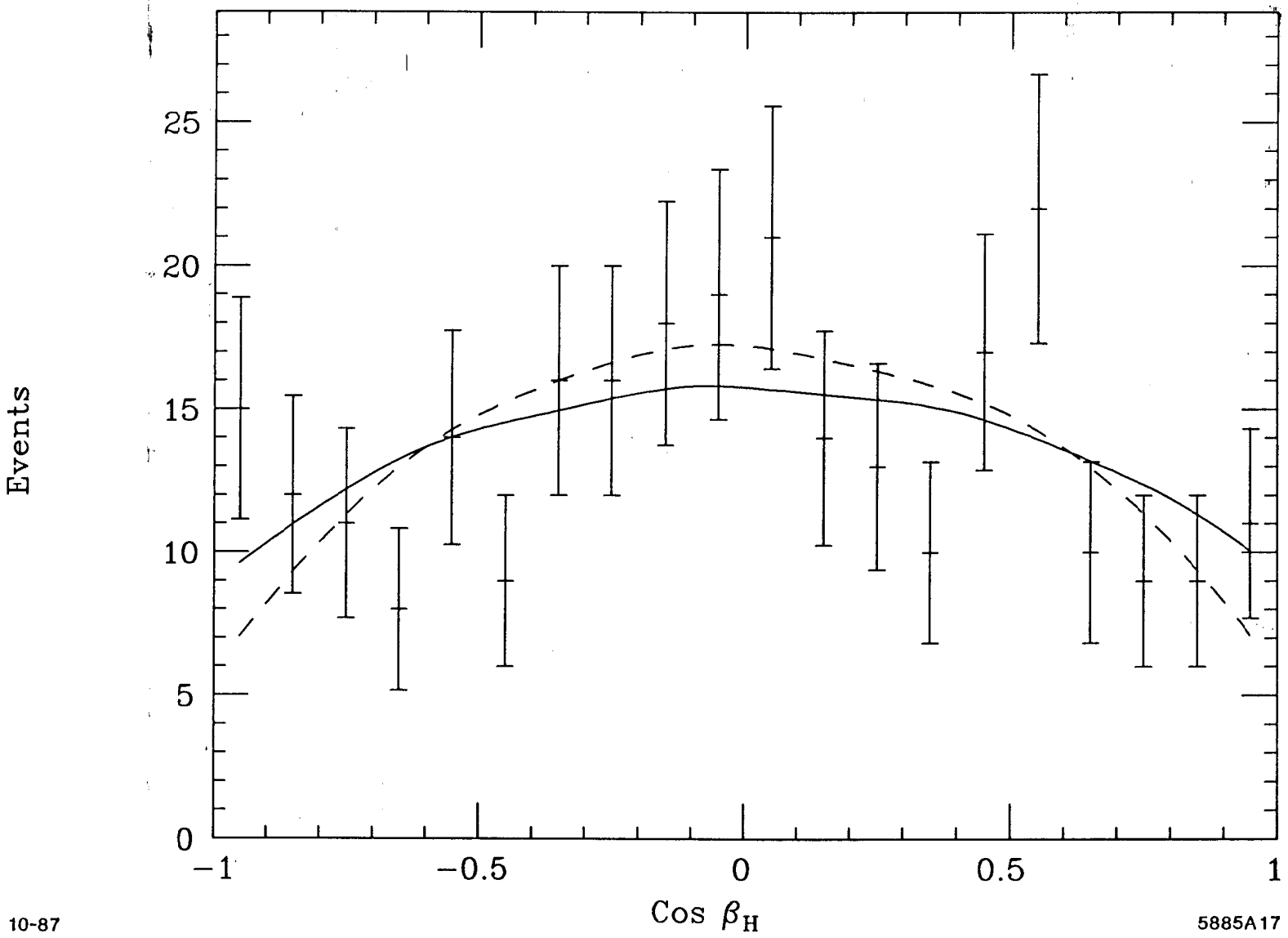

Figure 13e

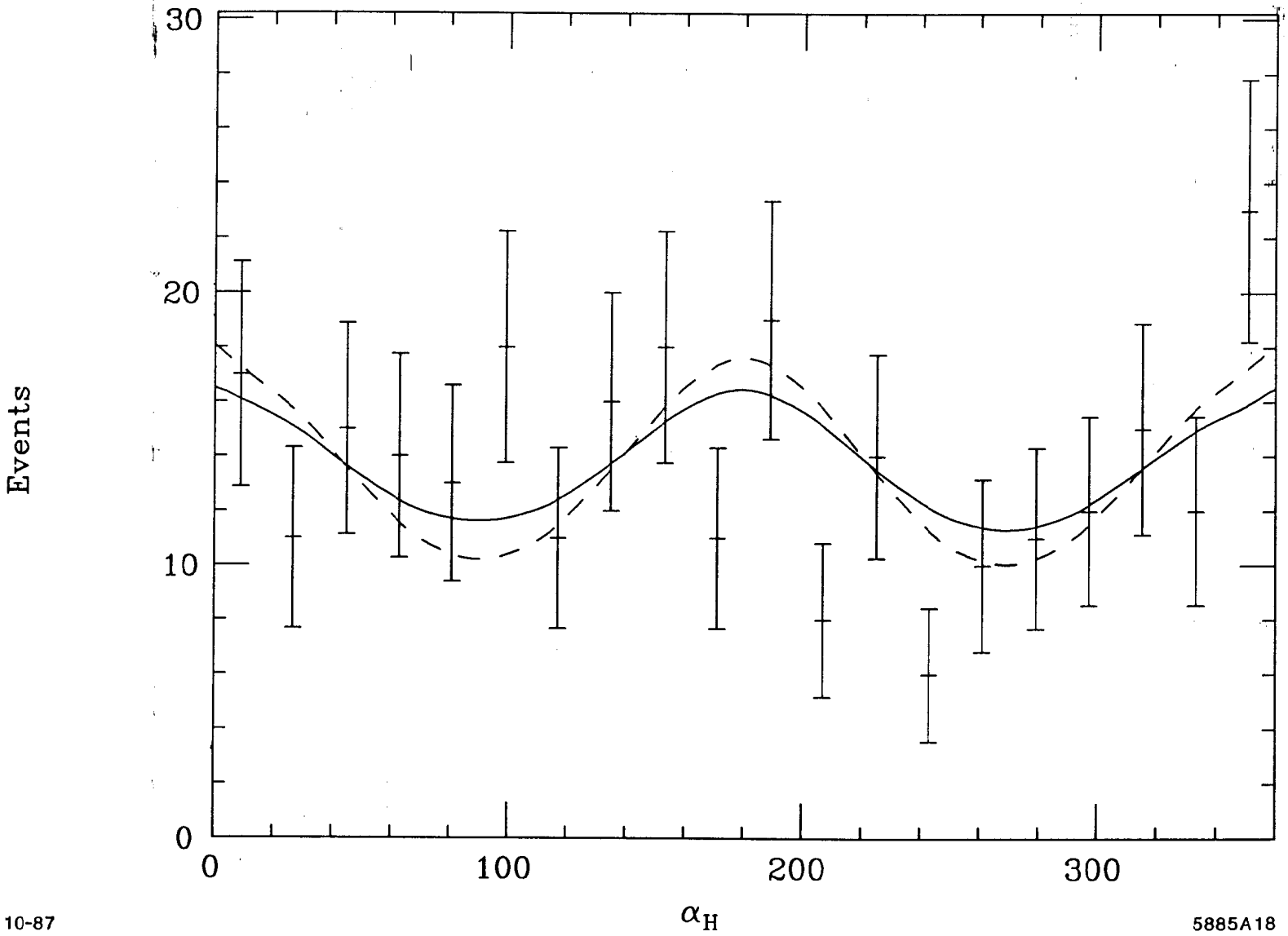

Figure 13f

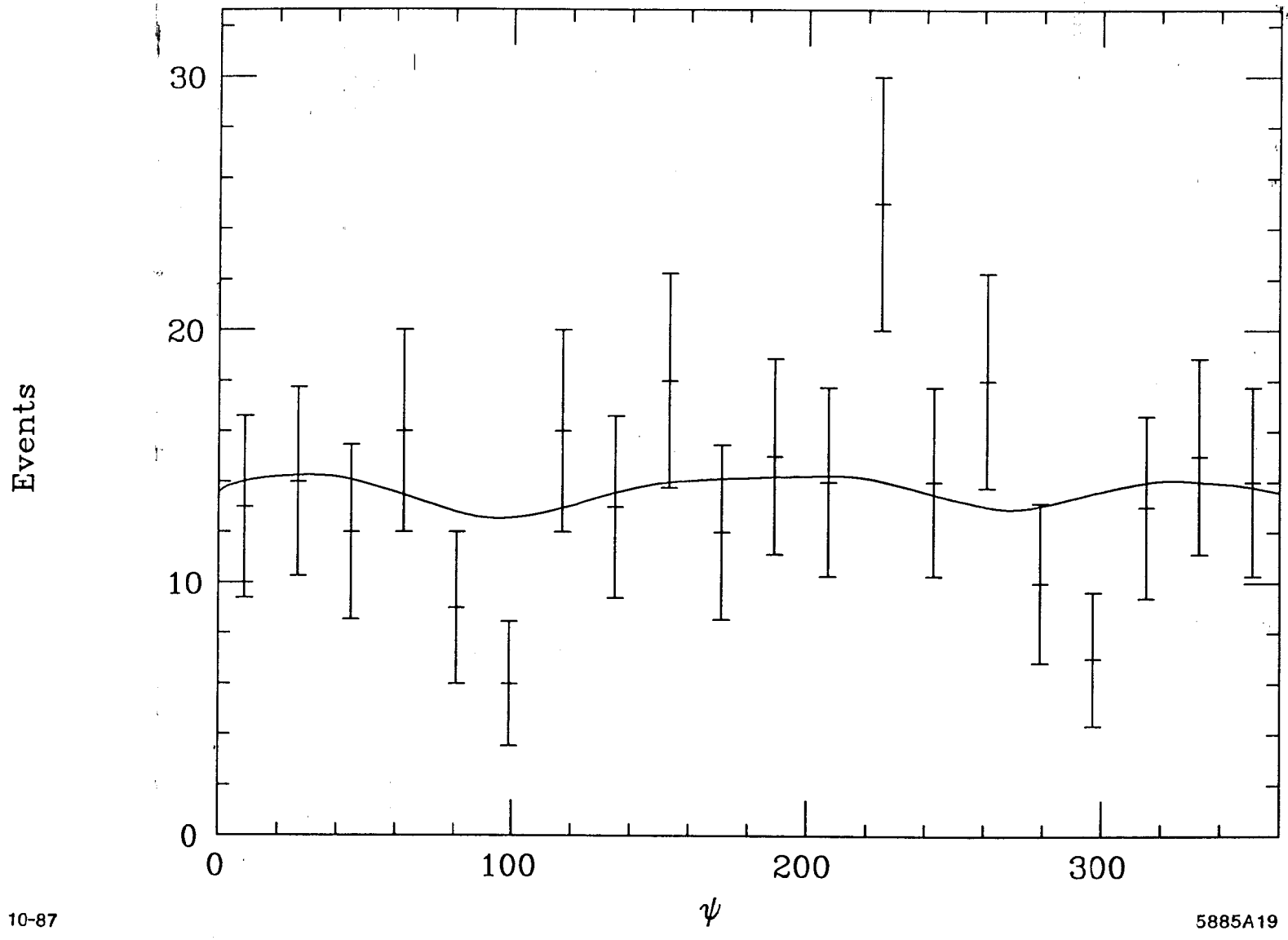

Figure 13g

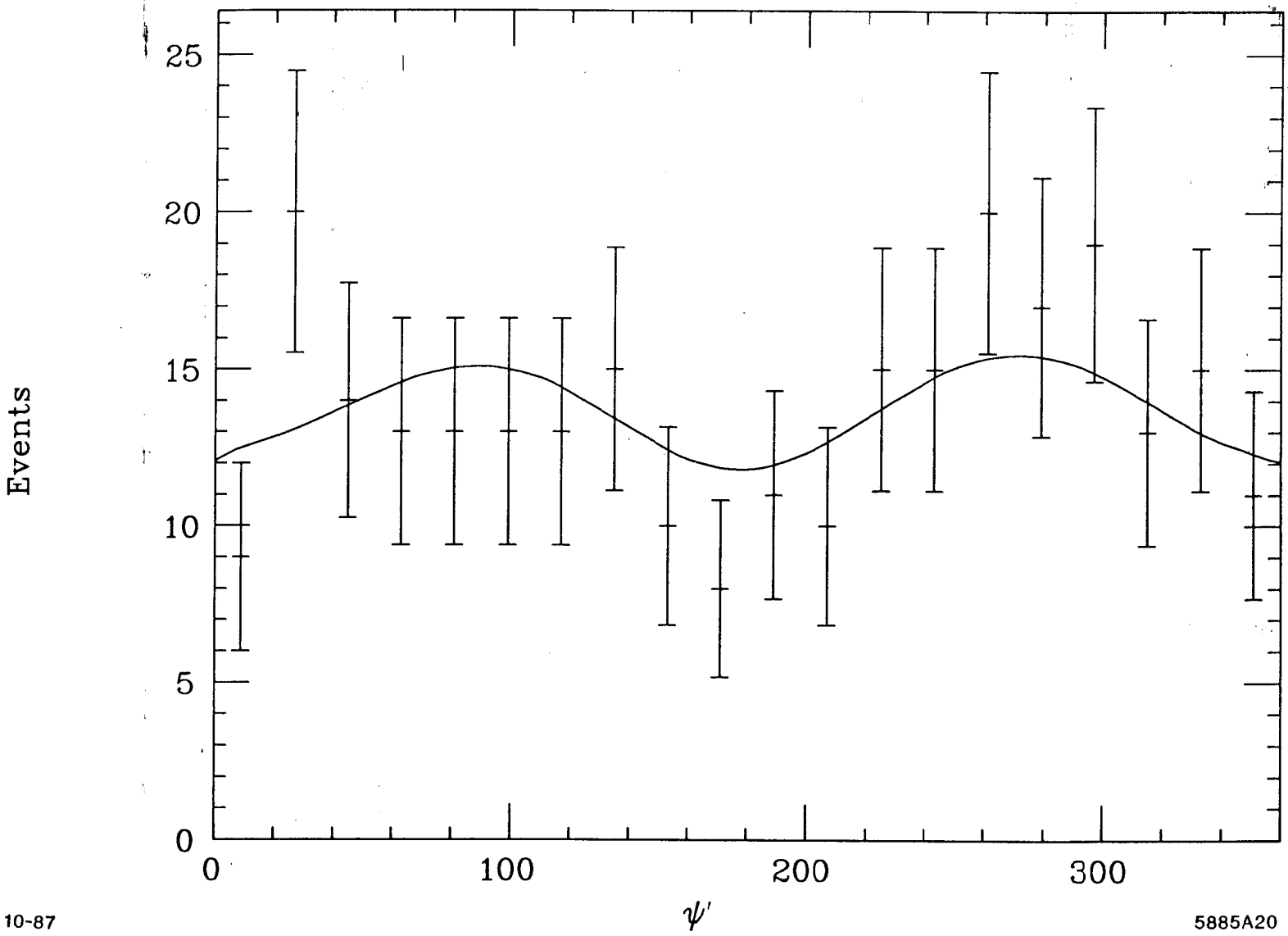

Figure 13h

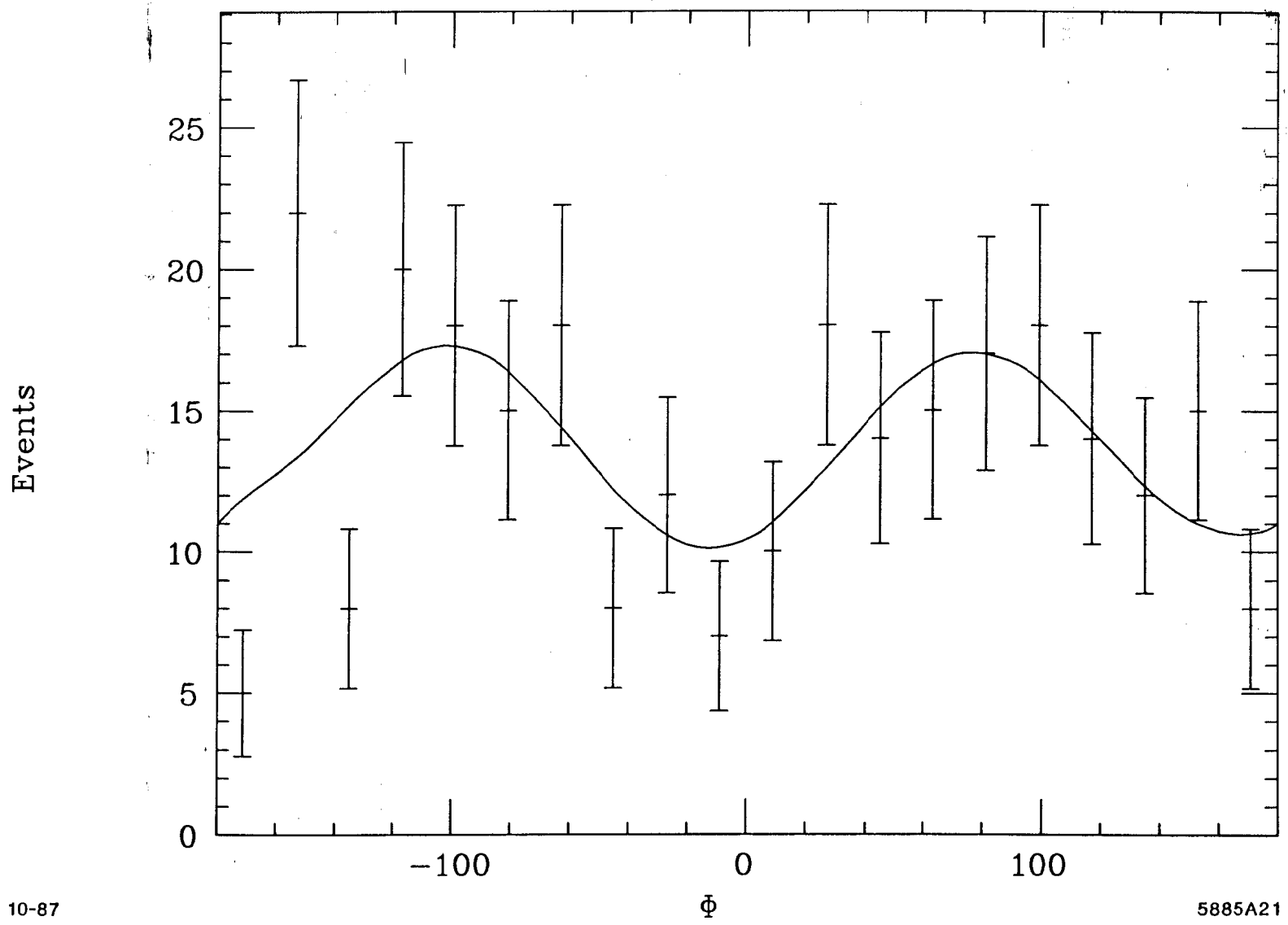

Figure 13i

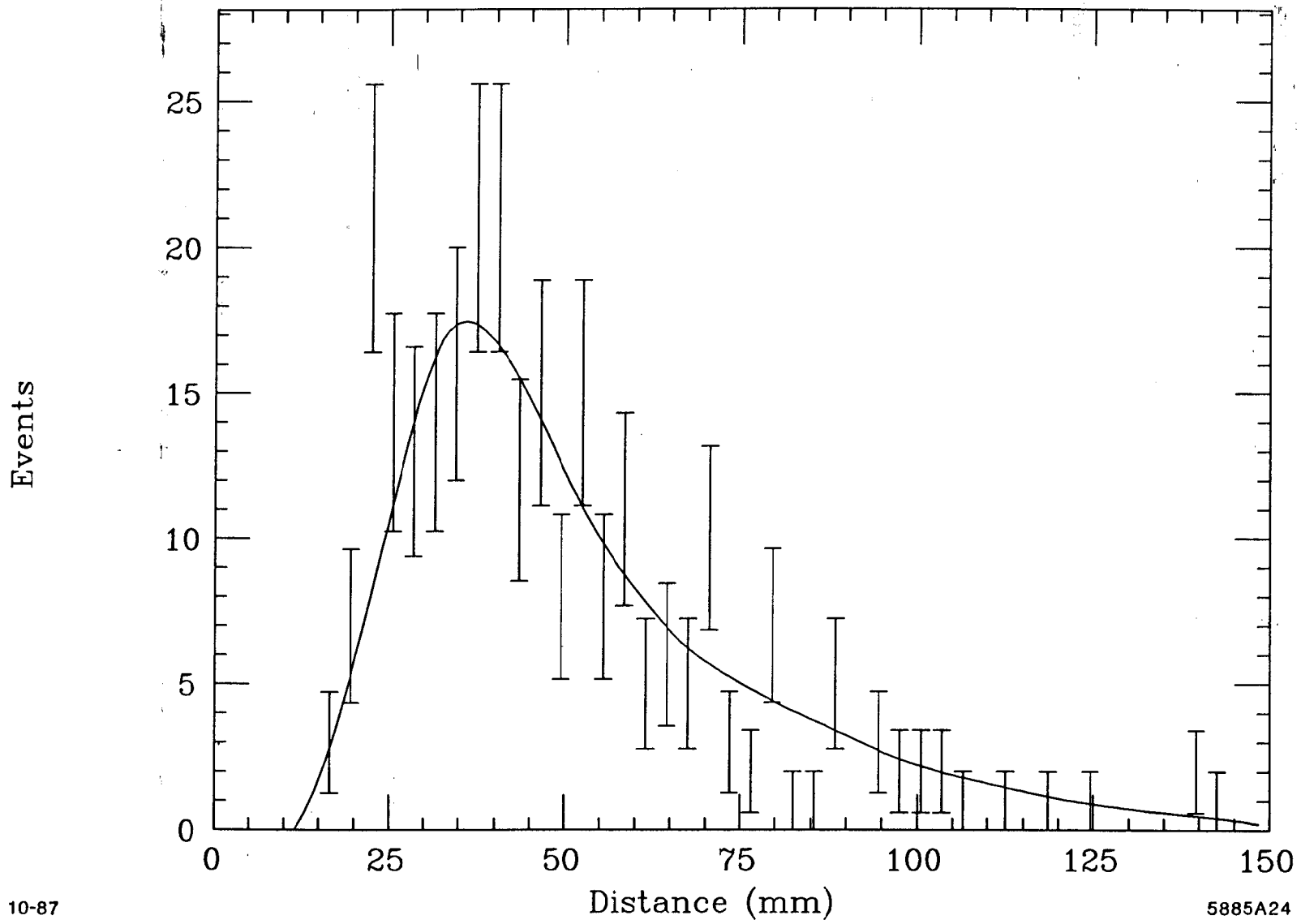
Events
25
20
15
10
5
0
0
25
50
75
100
125
150
Distance (mm)
10-87
5885A24

Figure 14

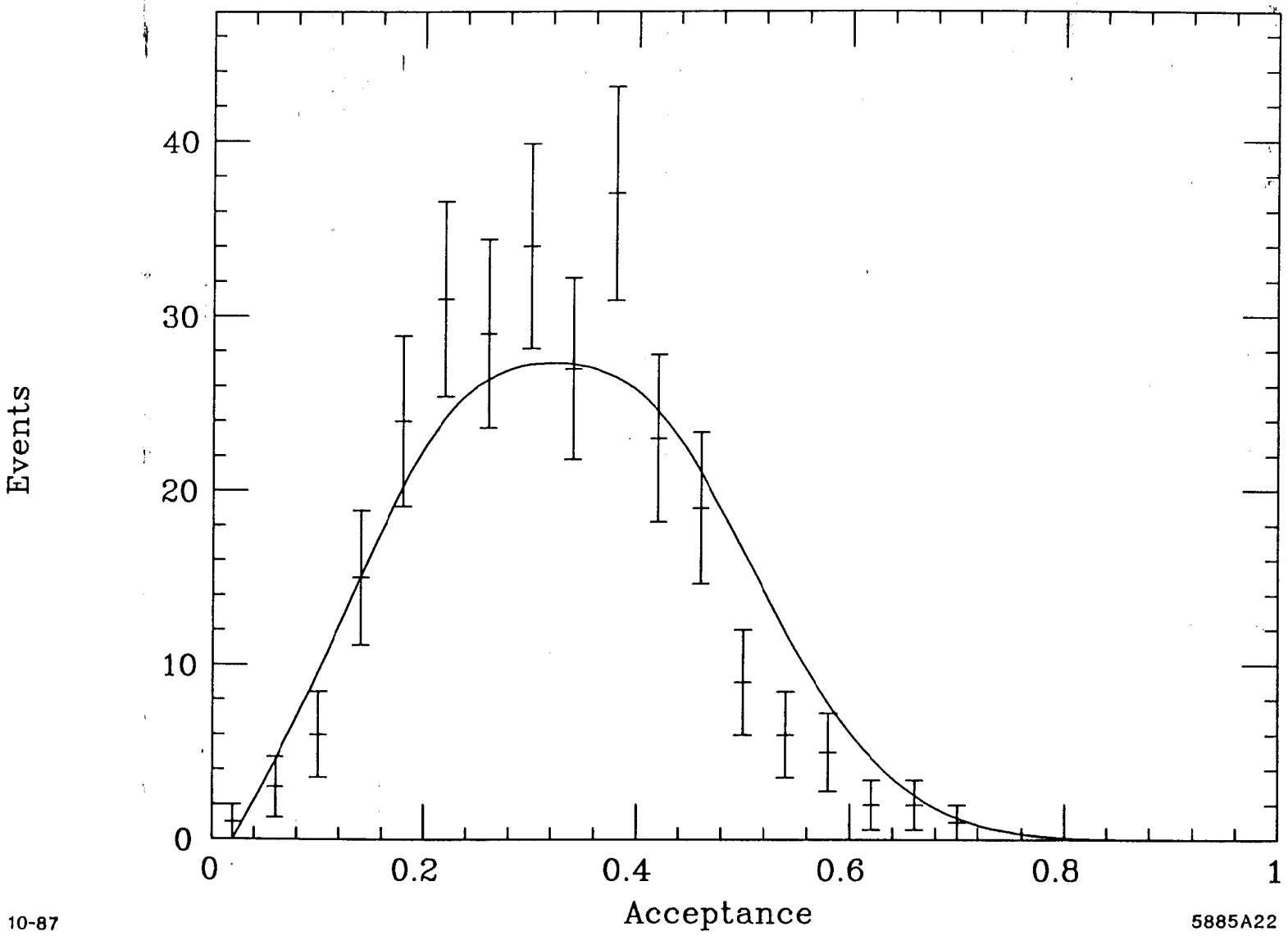

Figure 15

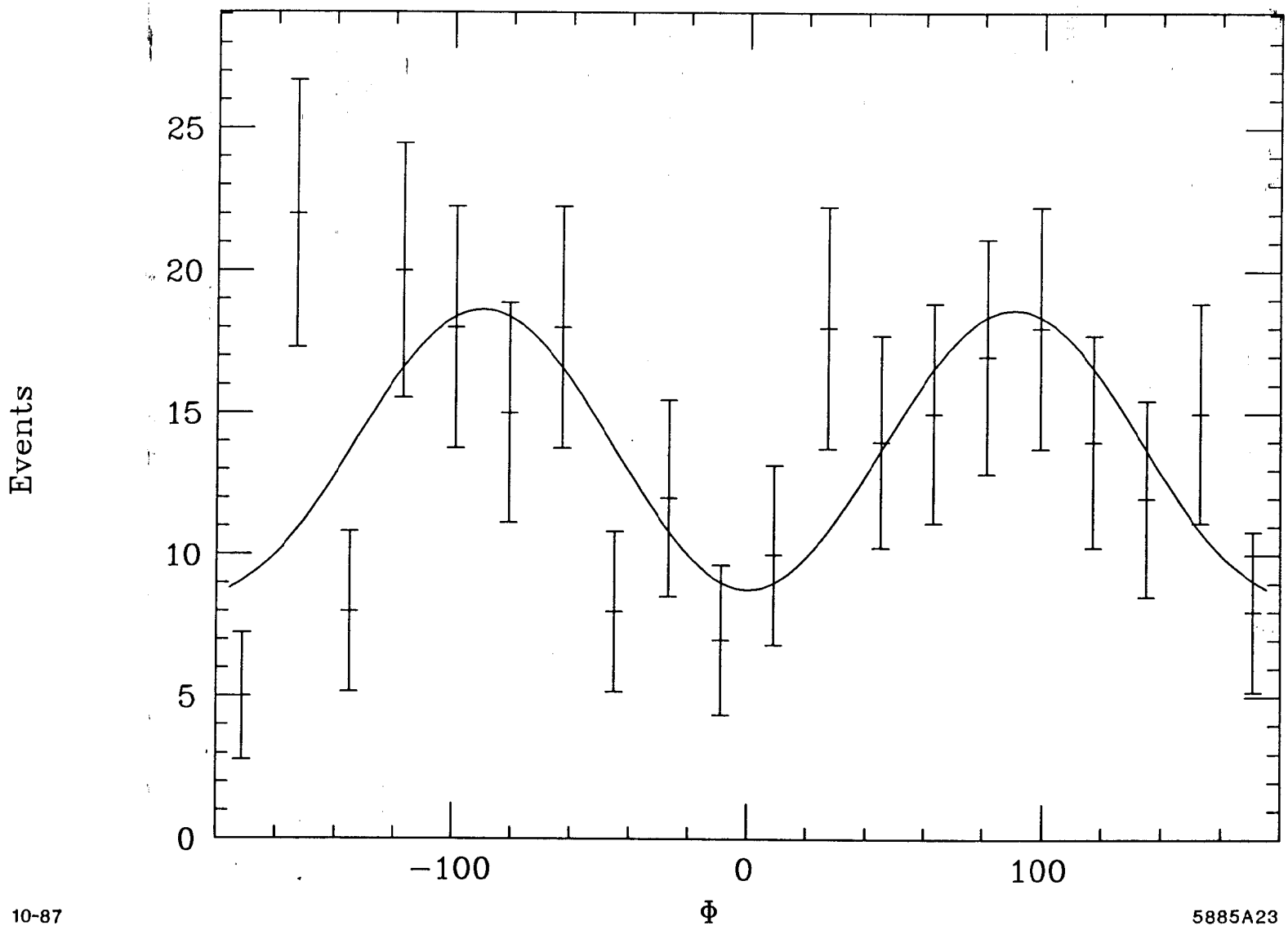

Figure 16

APPENDIX I

THE DETECTOR ACCEPTANCE

The acceptance for the experiment was determined by generating events according to the various models investigated and processing them through the simulation of response of the various detector subsystems. The simulation package (PEANUTS[13]) contains a detailed treatment of all the subsystems. In the case of the lead glass the measurements are treated in great detail, with all incident charged and neutral particles resulting in simulated photomultiplier pulse heights. These pulse heights are passed through the standard software used in the reconstruction of real data, so that all systematic effects that would thereby be produced are modeled. A record of reconstructed data is then available along with the original generated event to study the effects of the detector response. Again, the same software is used to find the $\gamma p \rightarrow p\omega^0\pi^0$ events in both the simulated data and the real data. Figures I-1 through I-9 show the angular distributions resulting from an isotropic decay. These curves resulted from running 100,000 events and show an average acceptance of 0.20.

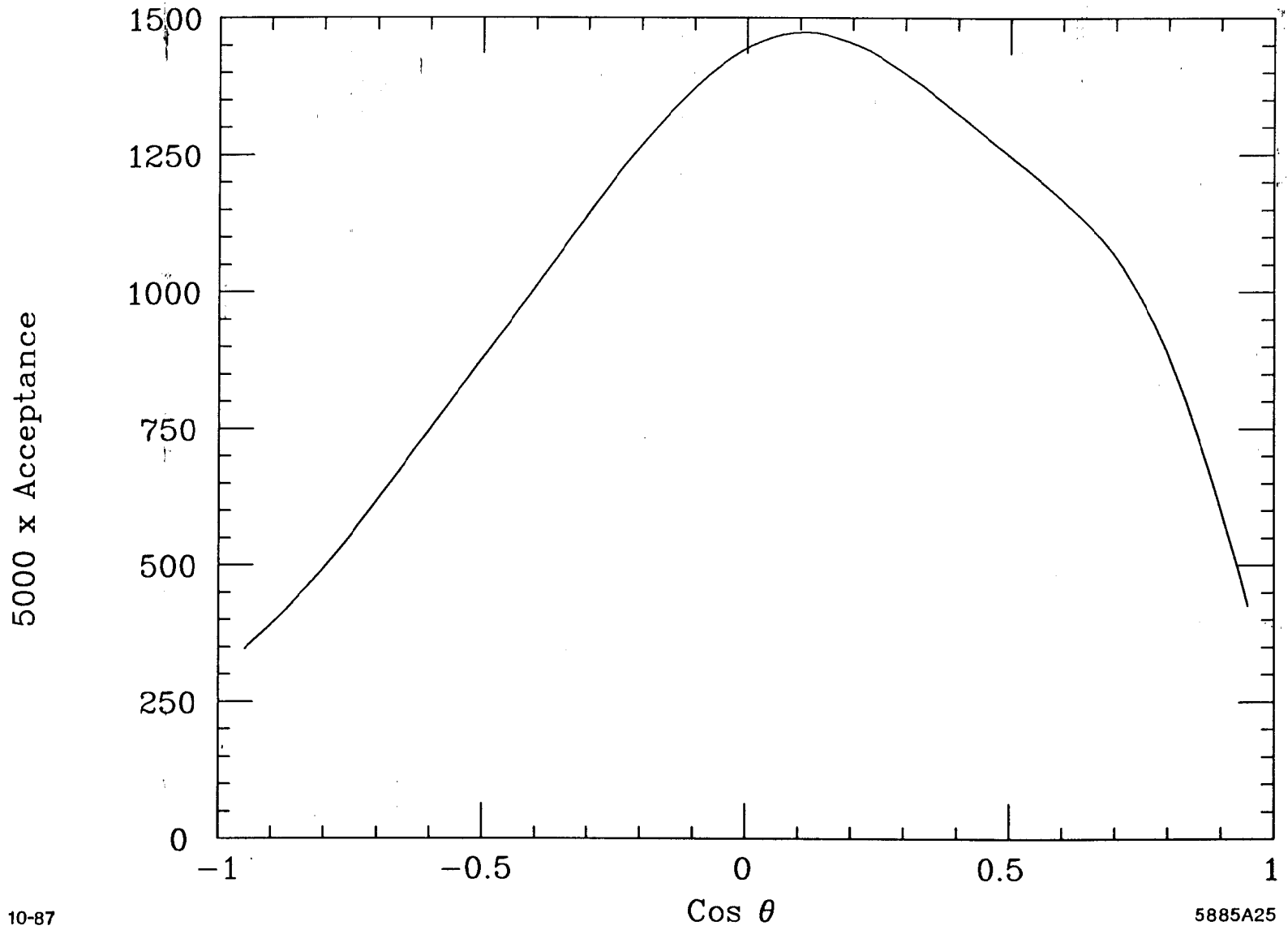
1500
1250
1000
750
500
250
0
5000 x Acceptance
−1
−0.5
0
0.5
1
Cos θ
10-87
5885A25

Figure I–1

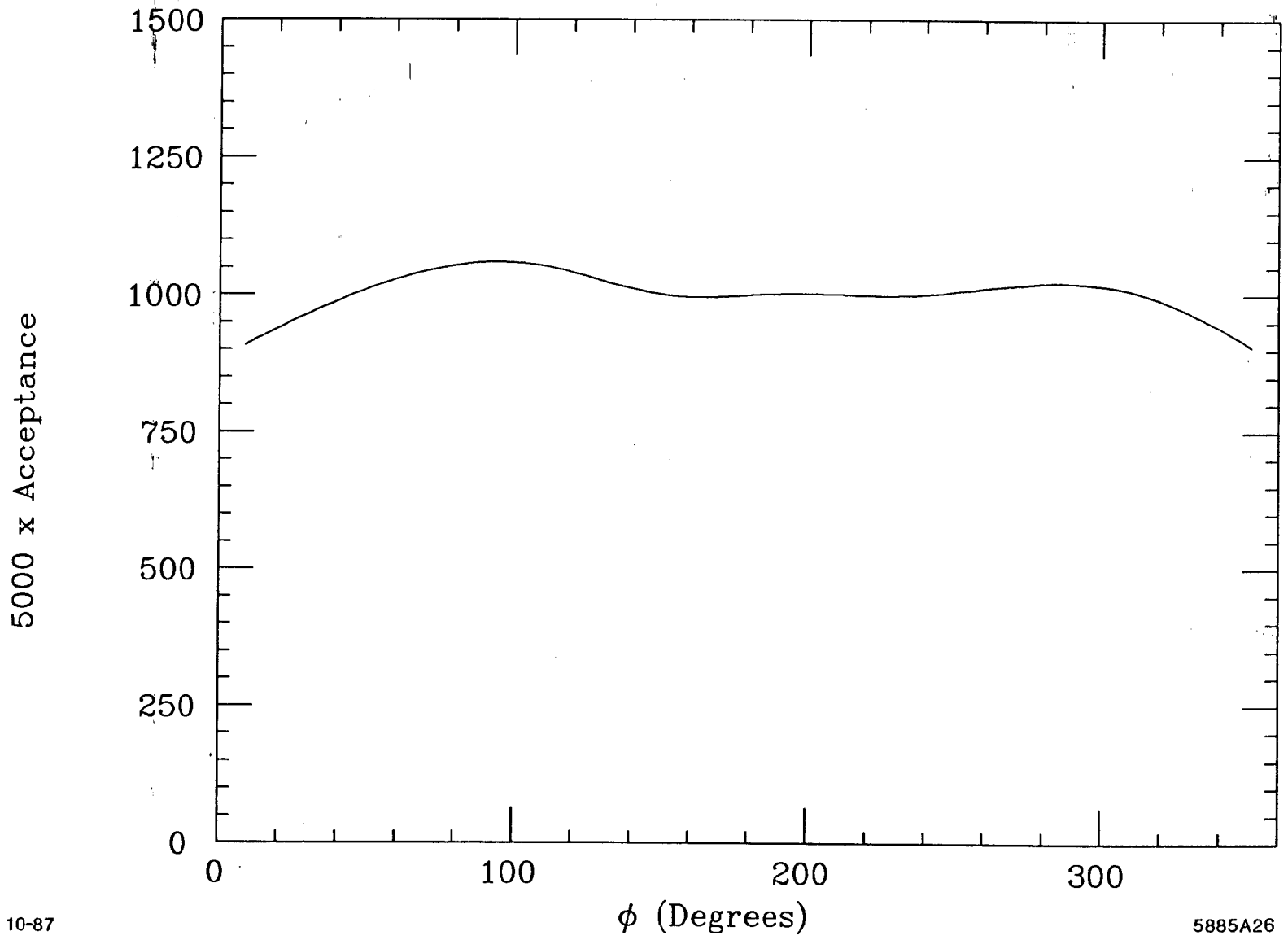
1500
1250
1000
750
500
250
0
5000 x Acceptance
0
100
200
300
ϕ (Degrees)
10-87
5885A26

Figure I–2

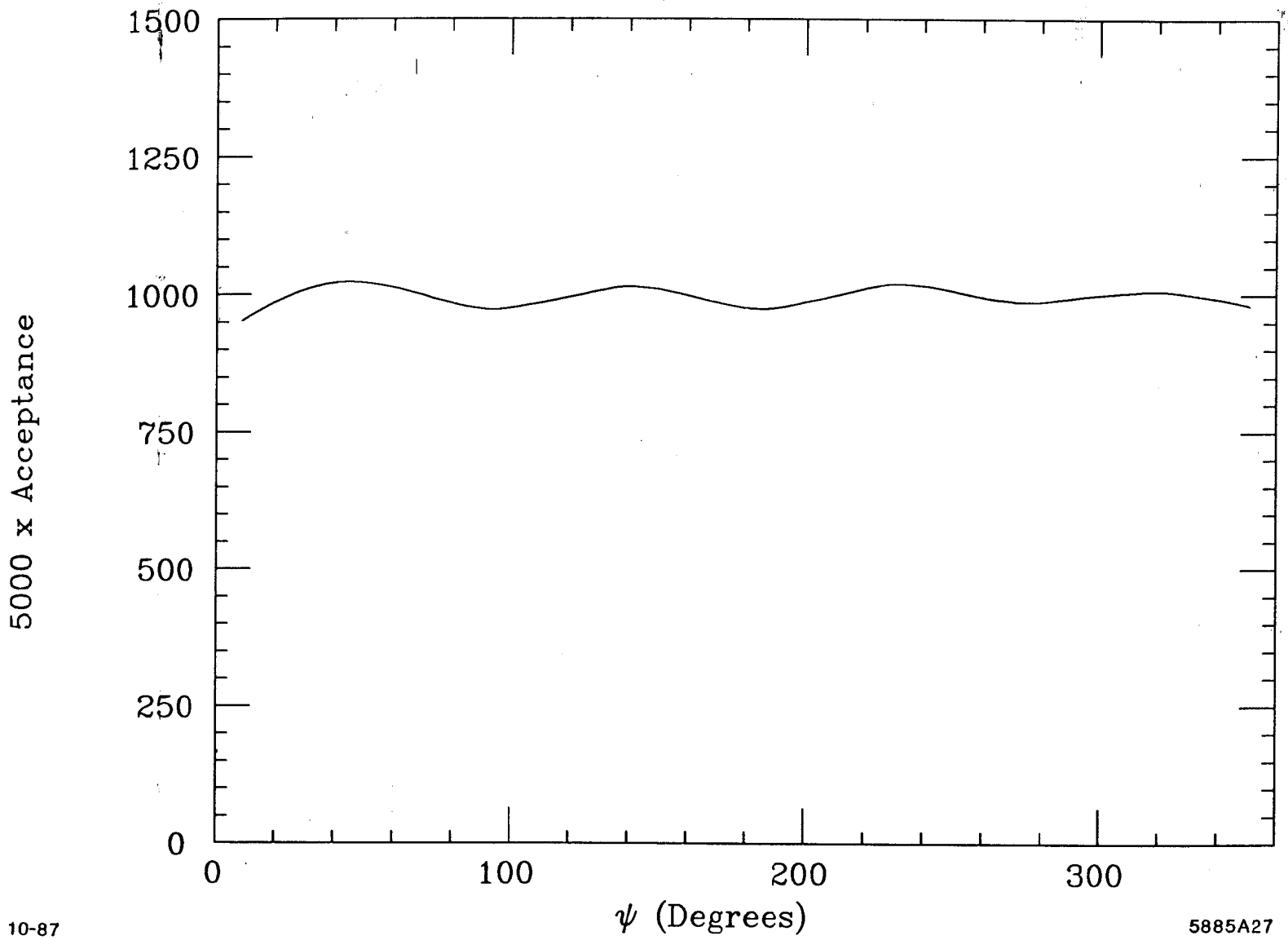
1500
1250
1000
750
500
250
0
5000 x Acceptance
0
100
200
300
ψ (Degrees)
10-87
5885A27

Figure I–3

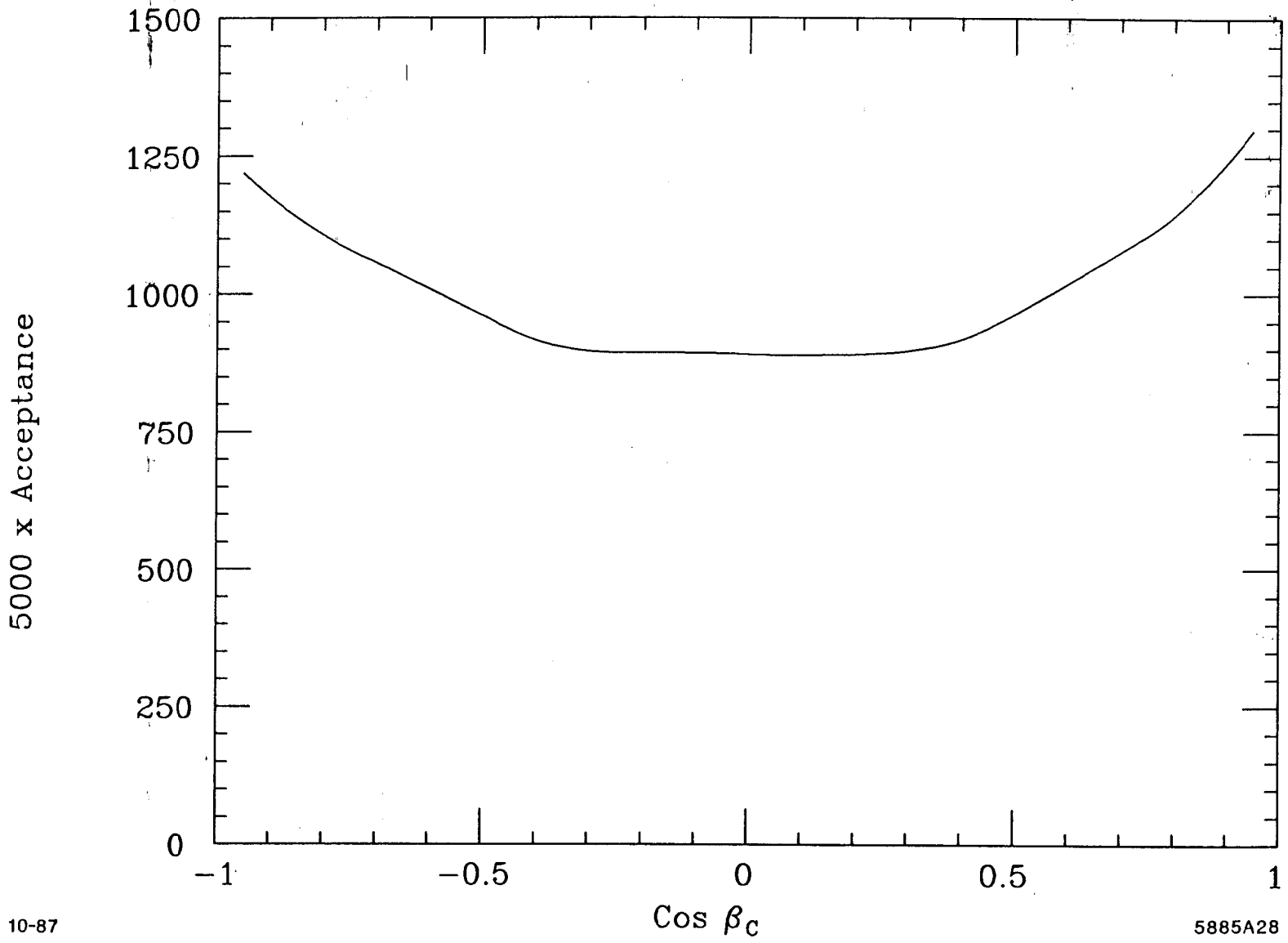
1500
1250
1000
750
500
250
0
5000 x Acceptance
−1
−0.5
0
0.5
1
Cos β_C
10-87
5885A28

Figure I–4

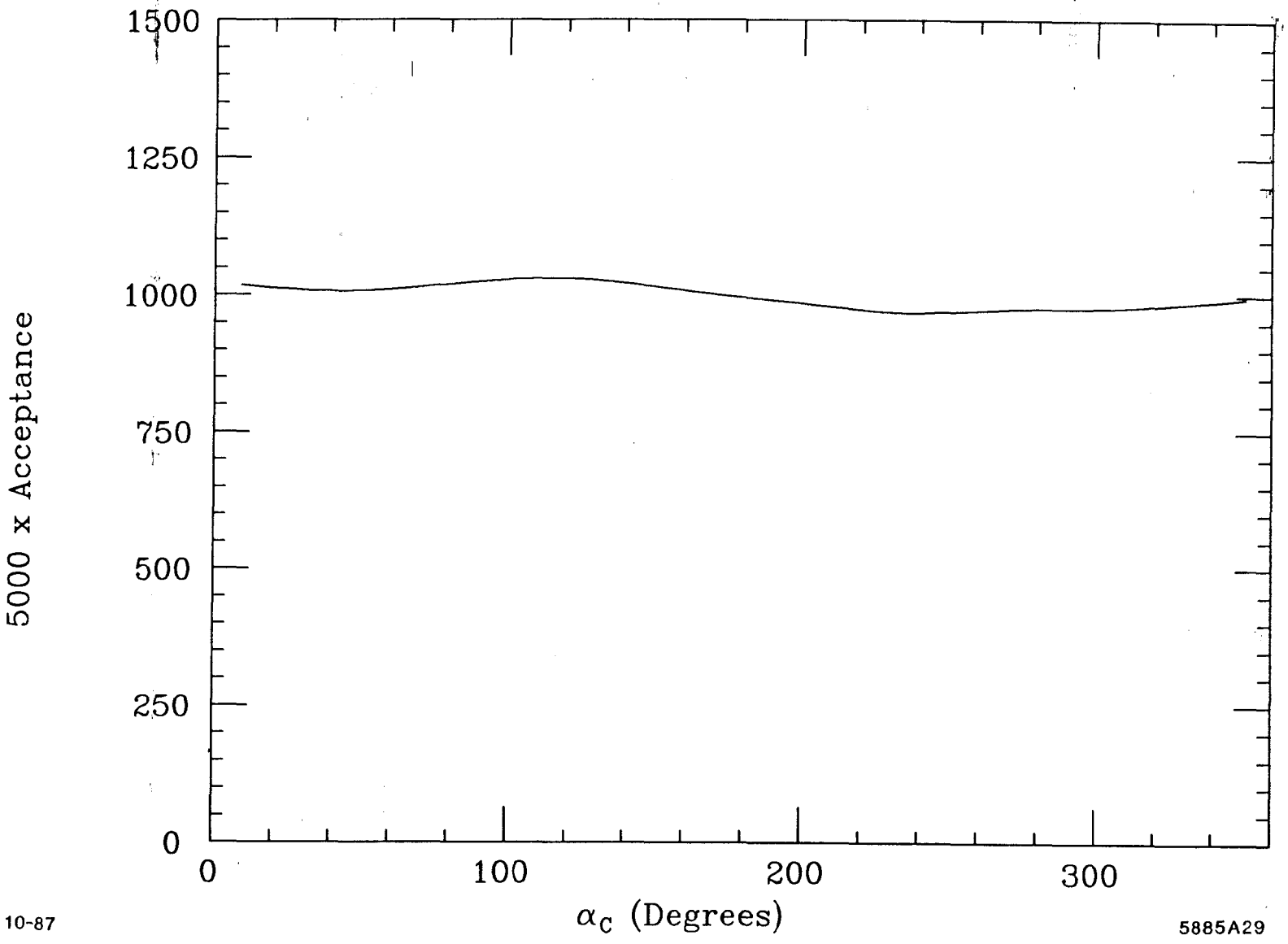
1500
1250
1000
750
500
250
0
5000 x Acceptance
0
100
200
300
α_C (Degrees)
10-87
5885A29

Figure I–5

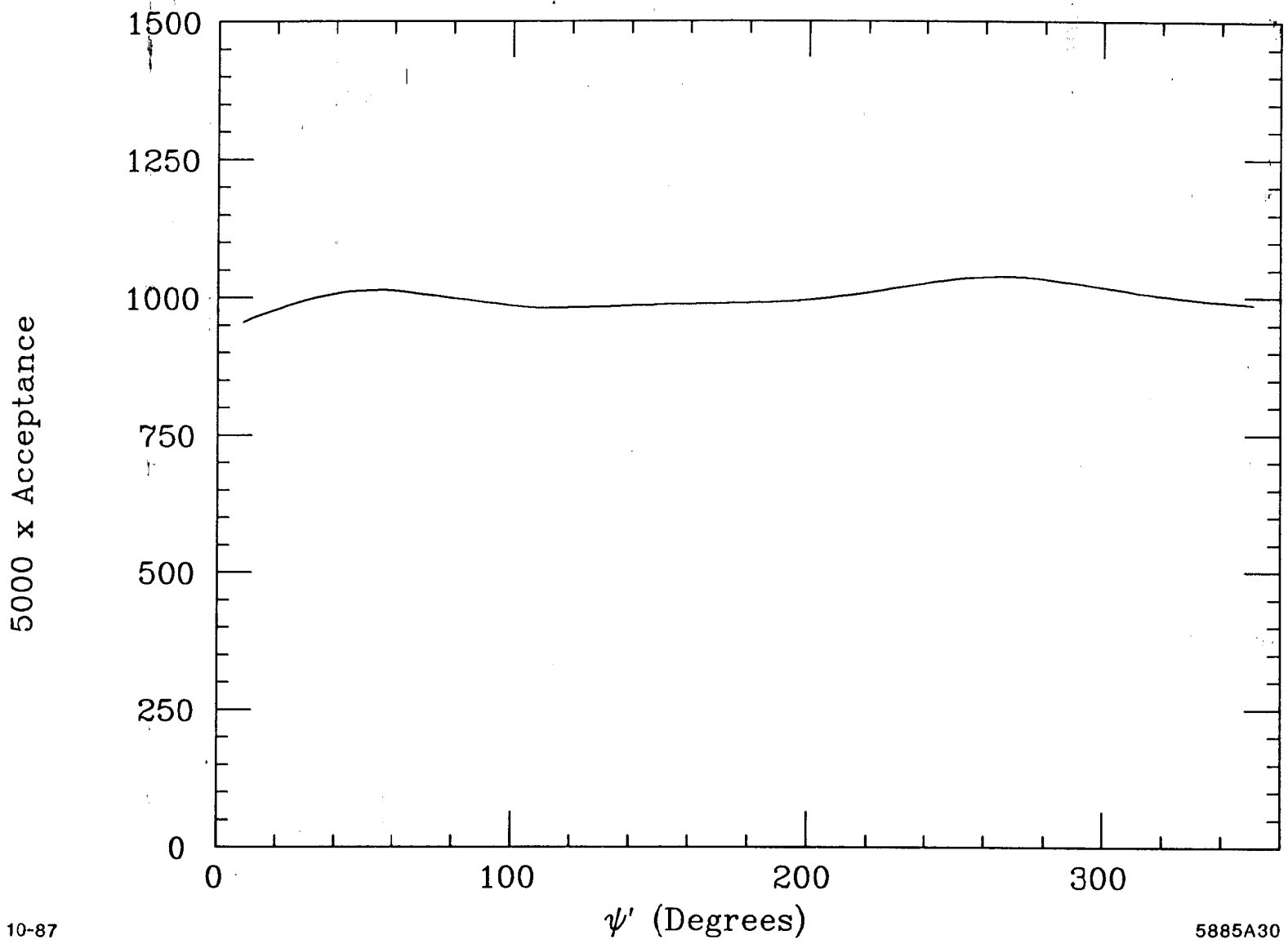
1500
1250
1000
750
500
250
0
5000 x Acceptance
0
100
200
300
ψ' (Degrees)
10-87
5885A30

Figure I–6

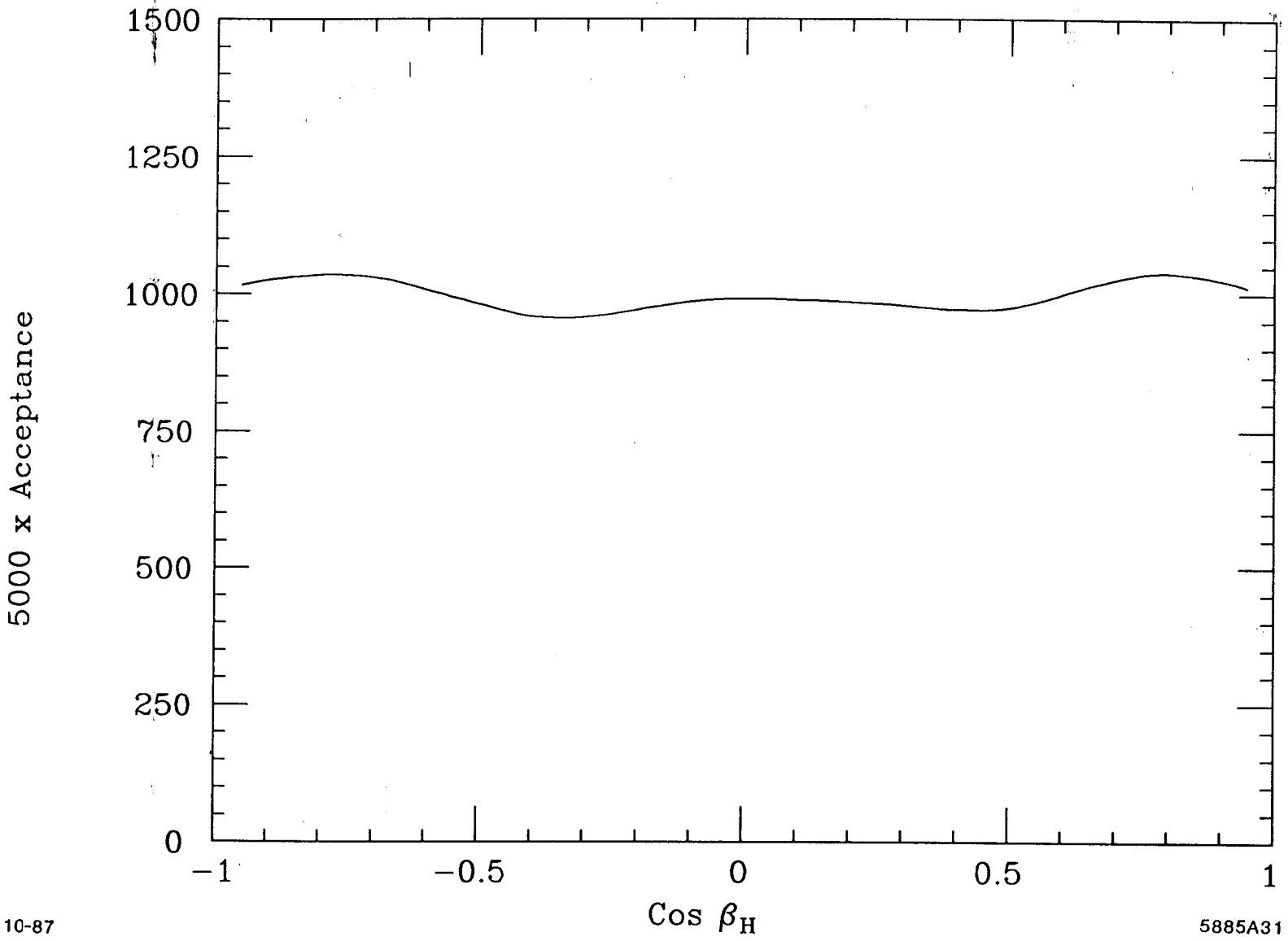
1500
1250
1000
750
500
250
0
5000 x Acceptance
−1
−0.5
0
0.5
1
Cos β_H
10-87
5885A31

Figure I–7

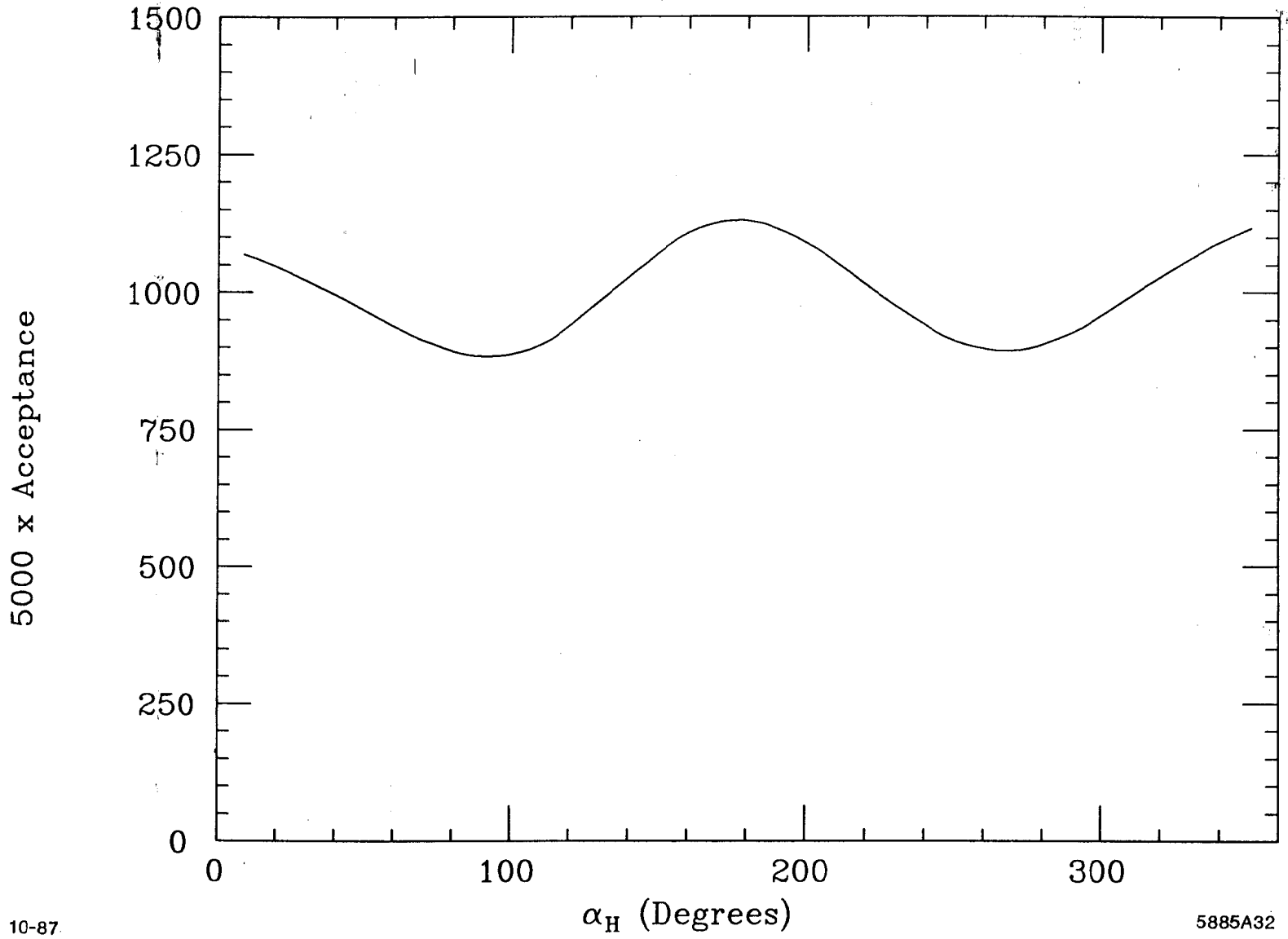
1500
1250
1000
750
500
250
0
5000 x Acceptance
0
100
200
300
α_H (Degrees)
10-87
5885A32

Figure I–8

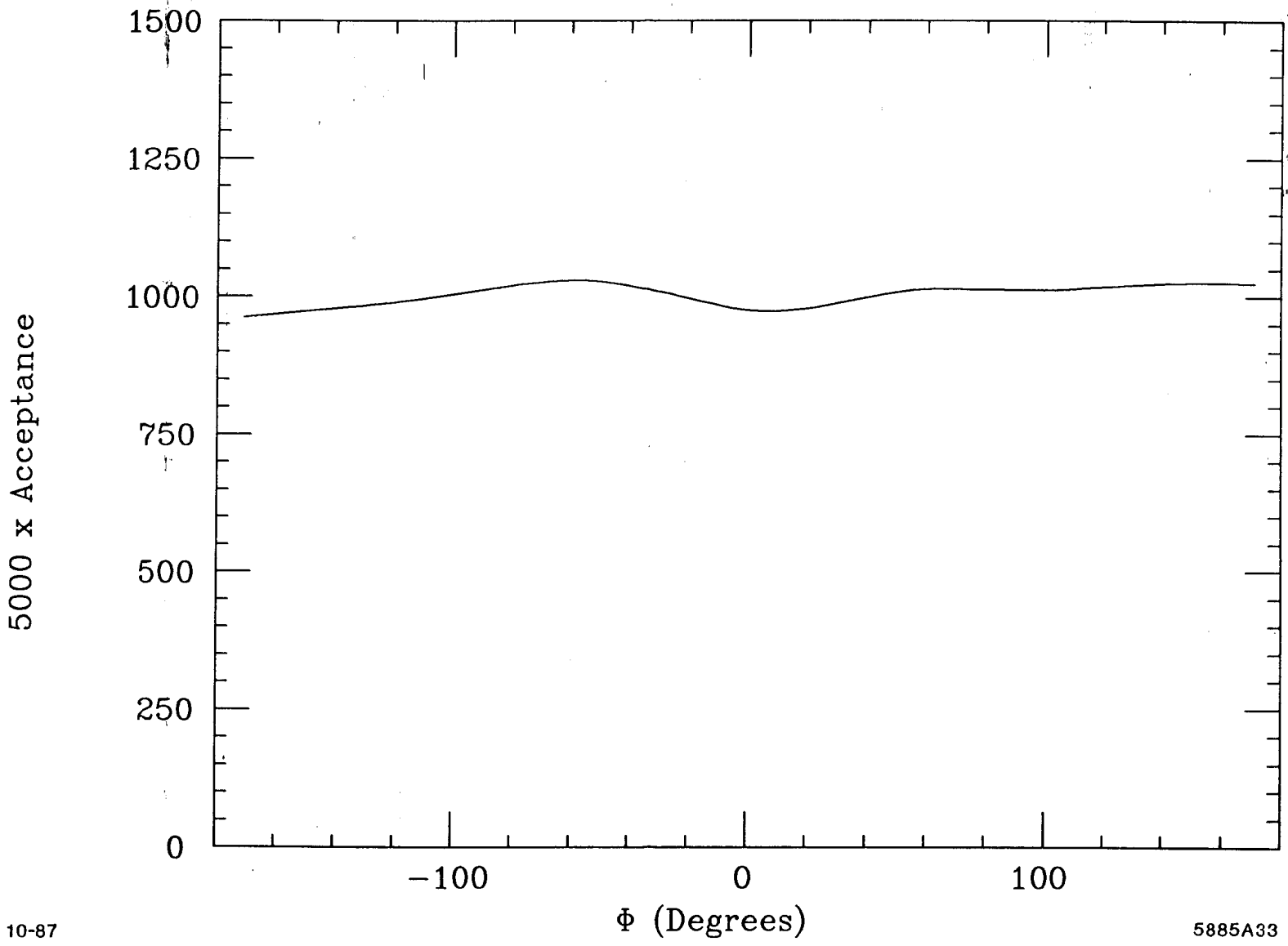
1500
1250
1000
750
500
250
0
5000 x Acceptance
−100
0
100
Φ (Degrees)
10-87
5885A33

Figure I–9

APPENDIX II

THE MOMENTS CORRECTION PROCEDURE

This appendix describes the procedure used to determine the moments: $H^{0\pm}_{s}(\alpha)$, $PH^{1\pm}_{s}(\alpha)$, and $PH^{2\pm}_{s}(\alpha)$. As described in the text, the angular distribution with respect to the angles $\Omega = (\cos\theta, \phi)$, $\Omega_H = (\cos\beta_H, \alpha_H)$, and Φ is parametrized as:

$$W = \frac{dN}{d\Omega\, d\Omega_H\, d\Phi} = \frac{N}{2\pi}(W_0(\Omega,\Omega_H) - PW_1(\Omega,\Omega_H)cos(2\Phi) - PW_2(\Omega,\Omega_H)sin(2\Phi))$$

$$W_k(\Omega,\Omega_H) = \sum_{\alpha} H^{k\pm}_{s}(\alpha) H^{\pm}_{\alpha}(\Omega,\Omega_H)/C_\alpha \qquad \alpha = lmLM$$

where the 25 orthogonal functions[15] $H^{\pm}_{lmLM}(\Omega,\Omega_H)$ (given in Table 1 of reference 8[18]) are related to the Wigner D functions by

$$H^{\pm}_{\alpha}(\Omega,\Omega_H) = \tfrac{1}{2}Re\{D^{L}_{Mm}(\phi,\theta,0)D^{l}_{m0}(\alpha_H,\beta_H,0) \pm (-1)^{L+M}D^{L}_{-Mm}D^{l}_{m0}\}$$

and $C_\alpha = (4\pi)^2/(2l+1)(2L+1)(2-\delta_{m0})(2-\delta_{M0})$.

We choose to work with the averages of the functions:

$$f^{0}_{\alpha} = H^{\pm}_{\alpha}(\Omega,\Omega_H),$$

$$f^{1}_{\alpha} = -H^{\pm}_{\alpha}(\Omega,\Omega_H)cos(2\Phi),$$

$$\text{and } f^{2}_{\alpha} = -H^{\pm}_{\alpha}(\Omega,\Omega_H)sin(2\Phi).$$

We can show that for perfect acceptance the averages of these functions:

$$< f^{i}_{\alpha} >= \frac{\int W f^{i}_{\alpha} d\Omega d\Omega_H d\Phi}{\int W d\Omega d\Omega_H d\Phi}$$

are related to the moments as follows:

$$H^{0\pm}_{s}(\alpha) =< f^{0}_{\alpha} >=< H^{\pm}_{\alpha}(\Omega, \Omega_H) >$$

$$PH^{1\pm}_{s}(\alpha) = 2 < f^{1}_{\alpha} >= 2 < -H^{\pm}_{\alpha}(\Omega, \Omega_H) cos(2\Phi) >$$

$$PH^{2\pm}_{s}(\alpha) = 2 < f^{2}_{\alpha} >= 2 < -H^{\pm}_{\alpha}(\Omega, \Omega_H) sin(2\Phi) > .$$

Since we do not have perfect acceptance we observe from our data

$$< f^{i}_{\alpha} >_{ob}= \frac{\int aW f^{i}_{\alpha} d\Omega d\Omega_H d\Phi}{\int aW d\Omega d\Omega_H d\Phi}$$

where $a(\Omega, \Omega_H, \Phi)$ is the acceptance. Now we define the average value for any function F to be

$$< F >_{mc}= \frac{\int aF d\Omega d\Omega_H d\Phi}{\int d\Omega d\Omega_H d\Phi}$$

which we can determine from the acceptance Monte Carlo. Notice that this average is normalized to the full phase space so that for $F = 1$ this is just the average acceptance (A).

We define as a condition of normalization $H_s^0(0000) = 1$. Now it can be shown:

$$(< f_\alpha^i >_{ob} < -cos(2\Phi) >_{mc} - < -cos(2\Phi) f_\alpha^i >_{mc}) P H_s^1(0000)$$

$$+(< f_\alpha^i >_{ob} < -sin(2\Phi) >_{mc} - < -sin(2\Phi) f_\alpha^i >_{mc}) P H_s^2(0000)$$

$$+ \sum_{\beta \neq 0} \sum_k (< f_\alpha^i >_{ob} < f_\beta^k >_{mc} - < f_\alpha^i f_\beta^k >_{mc}) P_k H_s^k(\beta)/C_\beta$$

$$= < f_\alpha^i >_{mc} - < f_\alpha^i >_{ob} A$$

(where $P_0 = 1, P_1 = P_2 = P$). From this set of equations we can easily obtain corrected values for the moments. We have checked our correction procedure by generating Monte Carlo events according to our obtained moments and applying this procedure to accepted Monte Carlo events.